Experiments on 2D Vortex Patterns in a Malmberg-Penning Trap with a Photocathode

by

Daniel Richard Durkin

B.A. (The Johns Hopkins University) 1990
M.A. (University of California at Berkeley) 1994

A dissertation submitted in partial satisfaction of the
requirements for the degree of
Doctor of Philosophy

in

Physics

in the

GRADUATE DIVISION
of the
UNIVERSITY of CALIFORNIA at BERKELEY

Committee in charge:

Professor Joel Fajans, Chair
Professor Jonathan Wurtele
Professor Alexandre Chorin

Fall 1998

The dissertation of Daniel Richard Durkin is approved:

Chair Date

Date

Date

University of California at Berkeley

Fall 1998

Experiments on 2D Vortex Patterns in a Malmberg-Penning Trap with a Photocathode

by
Daniel Richard Durkin

Abstract

Experiments on 2D Vortex Patterns in a Malmberg-Penning Trap with a Photocathode

by

Daniel Richard Durkin
Doctor of Philosophy in Physics

University of California at Berkeley

Professor Joel Fajans, Chair

The equations governing the evolution of a strongly magnetized pure electron system are analogous to those of an ideal 2D °uid; electron density is analogous to °uid vorticity. Therefore, we can study 2D vortex dynamics with pure electron systems in a Malmberg-Penning trap. We generate our electron systems with a photocathode, as opposed to the traditional thermionic sources. The photocathode provides increased control over the initial electron pro¯le, permitting us to perform previously inaccessible °uid-type experiments. The following results on the stability of 2D vortex patterns are presented here:

1. The stability of N vortices arranged in a ring.
2. The stability of N vortices arranged in a ring with a central vortex.
3. The stability of more complicated vortex patterns.

The electron pro¯le injected by an equipotential cathode is also investigated.

Professor Joel Fajans
Dissertation Committee Chair

To my parents,

Richard and Erma Durkin,

for all the love and support that made this thesis possible.

Contents

List of Figures

List of Tables

Acknowledgements

I came to Berkeley over 8 years ago, a naively con¯dent young man from the Maryland countryside. Not long after my arrival here, I was asked why I study Physics, a question to which I had never devoted much thought. A vision quickly came to mind of me as a young boy and my mother making a butter°y net and she setting me o® to chase the assorted insect life that inhabited the ¯elds of my home during the summer months. I'm really not just a physicist, but a scientist and a naturalist, and it is my mom whom I thank for starting me out on my pursuit of knowledge by pursuing a butter°y.

Along the way, though, I settled on experimental physics and that really means ¯xing computers, printers, mechanical pumps, magnets, power supplies, and even VCRs. The experimental physicist is in a constant struggle to have all their myriad equipment functioning at once. That moment is truly glorious and always elusive. I had no formal training in ¯xing these gadgets, but that never stops my father either. When something breaks, he calmly analyzes it, disassembles it, discerns it's inner workings, and ¯xes the damned thing. As he says, \if I can't ¯x it, it can't be ¯xed". So it was in the course of my research that when something broke, I often (though not always) calmly ¯xed the damned thing, and it is my father whom I thank for instilling this philosophy in me.

My parents also did not raise a quitter. The Photocathode Trap was an exercise in failure after failure, often of the bizarre. I so often wanted to walk away, but I would like to thank my advisor Joel Fajans for convincing me that failure was not an option and that success was close at hand.

My friends here at Berkeley have been invaluable. I would especially like to thank my fellow members of Project Mellon, Carl \Mr. Carl" Schroeder and Erik \Jiggy G" Gilson, for buoying me from drowning in the swirling seas of insanity with their good humor. I also thank Sharon Tiebert for her emotional and computer support. Tony Peurrung and John Notte took me under their wings when I joined this research group as a °edgling and both provided exemplary models of scientists that I have always tried to emulate.

The Berkeley Physics department is much more than faculty and students. It is also the ¯nest collection of support sta® essential to performing research. From ordering parts to putting those parts together to maintaining the electricity to make those parts do their thing, a research project is much more than a student and a theory. Thank you all.

So now it is that I leave Berkeley, 8 years older and a good measure wiser, con¯dent

in my abilities and aware of my inabilities, probably the greatest lesson I could ever hope to learn.

Chapter 1

Introduction

1.1 Background

The scientific method is founded upon the interplay between theory and experiment. Any theory that does not withstand the test of experiment must either evolve or it becomes extinct. This is not to say that experiment is master. Often experiments produce perplexing results that only theory can provide insight into and guide future studies. Theory and experiment must work in tandem for science to advance.

This is particularly challenging in fluid dynamics, and specifically two-dimensional (2D) fluid dynamics. 2D fluid dynamics is applied to flows where because of length scales, one dimension can be ignored and the system treated as essentially two dimensional. This idealization is applied to atmospheres and oceans, and a particularly noted example is Jupiter's Red Spot and its accompanying smaller vortex systems [1, 2, 3]. It is also used to understand phenomena in superfluids and superconductors.

2D fluid dynamics emerged from the effort to gain insight into real-world three-dimensional (3D) fluids. There has been intense theoretical effort, particularly in the areas of vortex dynamics and the evolution of 2D turbulence [4, 5, 6, 7, 8]. "Real" 2D fluids, though, are difficult to manipulate, difficult to diagnose, hindered by 3D boundary effects, and are perturbed by viscosity [9]. For these reasons, theory has far outpaced experiment. Predominantly, the experiments that could be performed were computational.

Electron systems in Malmberg-Penning traps [10, 11] provided a valuable experimental tool to test 2D fluid theories and close the gap that had separated theory and experiment. Two examples are the experiments on the Kelvin-Helmholtz Instability, also

referred to as the Diocotron Instability [12] (see Figure 2.12), and the merger of two symmetric vortices, also known as the Pairing Instability [13] (see Figure 2.13). These experiments are extremely difficult to perform with real fluids, primarily because of the difficulty in generating the initial vorticity profile.

Traditionally, Malmberg-Penning traps have used tungsten filaments as the electron source and this limits the initial electron profile (analogous to the fluid vorticity profile) to a circle. These circular electron columns can be manipulated by hollowing or chopping to perform the above mentioned experiments, but little more than that. The type of experiments that could be performed was unfortunately limited by the filament electron source.

With the following mandate, I began my graduate student research: to find a more flexible electron source to inject more complicated electron profiles and hence to perform previously inaccessible fluid-type experiments. The source that I settled on was a photocathode. Light shining on this photoemissive material would emit electrons; therefore, to inject a given electron profile, a light image of this profile would illuminate the photocathode and electrons corresponding to this image would stream into the trap.

The photocathode has greatly extended the range of fluid-type experiments that could be performed in a Malmberg-Penning trap. Experiments on the stability of 2D vortex patterns is the central contribution of this thesis. The majority of prior research on these patterns has been computational [14, 15]. These patterns are indeed impossible to controllably create in a real fluid, though they have been observed in superfluid helium [16, 17] and in electron plasmas [18]. In those systems, though, experimenters had extremely limited control over the initial electron profile. The photocathode provided me with the control that was previously lacking. For the first time experimentally, complicated 2D vortex patterns were controllably created and studied.

The photocathode has also opened the door to a whole slew of fluid-type experiments that could now be performed in a Malmberg-Penning trap:

- The dependence of the stability of N vortices arranged in a ring with a boundary on the ring radius [19]. It was a goal of this thesis to perform this experiment, but nonuniform emission of the photocathode at larger radii made it impossible.

- The formation of vortex crystals. The \cooling" of unstable vortex patterns into stable patterns has been observed in superfluid helium [16, 17] and in a Malmberg-Penning trap with electrons [18]. In the superfluid helium, interaction of the superfluid with the

normal component provides a cooling mechanism. In our pure electron systems, the cooling mechanism is not well understood, but may be due to the vortices interacting with a weak electron background [20].

- The decay of 2D turbulence [21, 22, 23]. The evolution of 2D turbulence involves the formation of vortices that subsequently merge or are sheared away. Scaling theories have been developed to predict how the number of vortices decays with time [24, 25, 26, 27, 28, 29, 30]. Experiments have been performed in electrolytic solutions, but su®er from viscosity and report con°icting results [31, 32]. An experiment has also been performed in a Malmberg-Penning trap, but with limited control over the initial conditions [18].

- The merger of two asymmetric vortices [33, 34, 35]. Symmetric vortex merger has been studied in a Malmberg-Penning trap at UCSD, but because of the limited control over the initial conditions with their thermionic source, it was di±cult to extend to the case of asymmetric vortex merger [36].

- \Negative" vorticity. A criticism of performing °uid-type experiments in a Malmberg-Penning trap is that because we trap only electrons, there is only one sign of vorticity. A possible solution to this is the behavior of a \hole" in a uniform background of electrons [37]. Here, a transformation to the rotating frame should also transform the hole to the opposite sign of vorticity. To have both signs of vorticity, consider a uniform background of density n, a hole acting as one sign of vorticity, and a column of density 2n acting as the other sign.

- The Love Instability: the dependence of the stability of an elliptical vortex on ellipticity [38].

The photocathode, though, has proven to be a mixed blessing. It was extremely challenging to incorporate into a Malmberg-Penning trap, primarily because it needed to be fabricated in situ, within the vacuum chamber. Most of my research e®ort focused on this fabrication process, a process that bordered on black magic at times. Now, after a great deal of e®ort, the process has become reproducible and the only obstacle to performing the above listed experiments has been removed. This, I hope, will bene¯t the next generation of graduate students.

1.2 Outline

This thesis is outlined as follows:

- Chapter 2 The Experimental Apparatus: The Malmberg-Penning trap used to perform these experiments is described. Special attention is given to the photocathode that made the 2D °uid-type experiments possible.
- Chapter 3 The Equipotential Cathode: The performance of an equipotential photocathode is examined. It is shown to be superior to traditional thermionic electron sources, at least in the regime of injecting electron systems on the order of a Debye length in radius.
- Chapter 4 Experiments on 2D Vortex Patterns: The stability of 2D vortex patterns is examined using electron columns injected from a photocathode. These experiments would have been extremely di±cult, if not impossible, to perform in a real °uid and even in a Malmberg-Penning trap without a photocathode.
- Appendix A The Fluid Analogy: The analogy that permits me to use my electron trap to perform 2D °uid-like experiments is presented.
- Appendix B Magnetic Field Alignment Procedure: It is important to have the magnetic ¯eld aligned with the trap's axis. The photocathode allows for a unique alignment procedure that is outlined here.
- Appendix C Electric Potential Pro¯le Control Option for the Photocathode: Though the equipotential photocathode has proven to work well and is able to perform a number of experiments, the option to control the electric potential across the surface may be needed in the future. Here, the option that was developed in the course of this research is presented.

Chapter 2

The Experimental Apparatus

The experimental apparatus is generically referred to as a Malmberg-Penning trap [10, 11]. I will refer to the one speci¯cally used for this thesis research as The Photocathode Trap. It features a photocathode electron source, allowing for the controlled injection of more complicated electron pro¯les over previously used thermionic sources. The main diagnostic is an imaging system that uses a phosphor screen and a CCD camera.

The Photocathode Trap is in many ways a throwback to simplicity. Machines had become increasingly complicated as °exibility often drove their design. The return to simplicity was necessitated by the development of the photocathode electron source. The photocathode is a new technology in the ¯eld of Nonneutral Plasma Physics and its development required frequent vacuum breaks, which in turn necessitated a machine that could be quickly and easily opened, cleaned, reset, and then pumped back down again. Unfortunately, this lesson was not learned until after a very complicated, though °exible, trap was constructed. That trap now sits idle.

2.1 The Trap

The Photocathode Trap is a Malmberg-Penning trap. It consists of electrically conducting con¯nement gates immersed in an axial magnetic ¯eld and contained within an ultra high vacuum chamber.

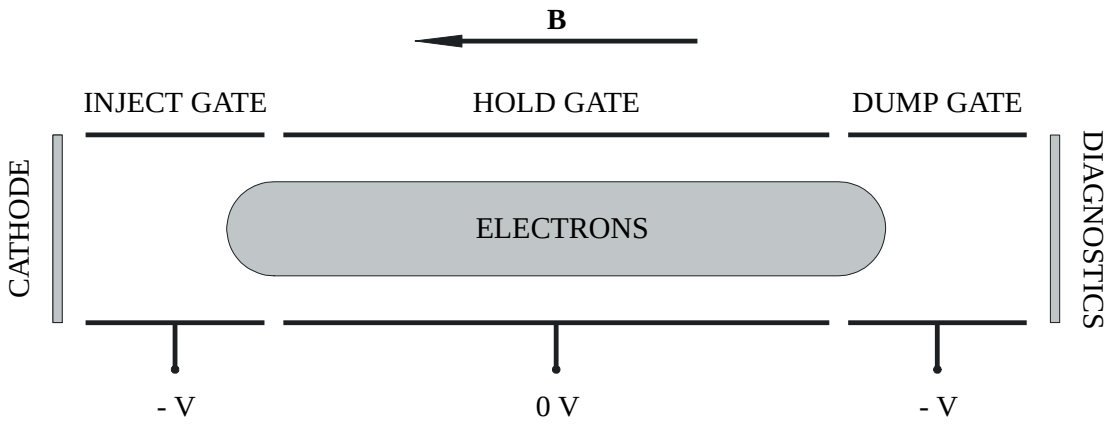

Figure 2.1: Side cross section of con¯nement region.

2.1.1 Malmberg-Penning Traps

A Malmberg-Penning trap uses static magnetic and electric ¯elds to trap electrons (generally, it will trap species of one sign of charge). The cross section of a generic Malmberg-Penning trap is diagramed in Figure 2.1. The trap consists of at least three coaxial conducting cylinders, commonly referred to as gates. The gates are contained within an high vacuum chamber. Radial con¯nement is provided by an axial magnetic ¯eld. The electrons gyrate about the magnetic ¯eld and if the ¯eld is strong enough, can be essentially considered pinned to the magnetic ¯eld lines. Axial con¯nement is provided by applying negative voltages to the end gates with respect to the central gate. Therefore, electrons are trapped bouncing back and forth between the end gates.

The trap is contained within an high vacuum chamber, because collisions with the background gas will limit the lifetime of the trapped electron system.

In the simplest trap, the three gates are referred to as the inject, hold, and dump gates. Electrons are trapped in the following manner (see Figure 2.2):

1. Inject: Initially, the inject and hold gates are grounded, and the dump gate is at a negative electric potential. Electrons are allowed to stream o® the cathode, along the magnetic ¯eld lines into the inject and hold gates, and then bounce o® the negative potential of the dump gate.

2. Hold: To trap the electrons, a negative potential is applied to the inject gate. Electrons will then be trapped in the hold gate, bouncing between the inject and dump

gates.

3. Dump: To release the electrons, the dump gate is grounded, allowing the electrons to stream out along the magnetic ¯eld lines. At this stage, the electrons are typically accelerated with electric ¯elds into a phosphor screen for imaging.

2.1.2 Con¯nement Gates

The Photocathode Trap consists of just three simple gates (see Figure 2.3), resting on alumina rods within a copper U-channel (see Figure 2.4):

- The inject and dump gates are both 4 times the inner radius in length. This is to guarantee that the electric potential at the center of the gate is the same as the potential applied to the gate itself.
- The hold gate is 10 times the inner radius in length. This is to minimize ¯nite length e®ects, as characterized by Kevin Fine [39], that modify the diocotron frequency:

$$\epsilon_{infinite} = \left(1 + \left(1.3 - 1.08\frac{R_p}{R_w}\right)\left(\frac{R_w}{R_p} - \frac{R_p}{R_w}\right)\left(\frac{R_w}{L_p}\right)^2\right)\epsilon_{finite}; \qquad (2.1)$$

  where $\epsilon_{infinite}$ is the theoretical in¯nite length diocotron period, ϵ_{finite} is the measured ¯nite length diocotron period, R_w is the gate's wall radius, R_p is the electron column's radius, and L_p is the electron column's length.

- The gates are separated by alumina spacers that translate into a 0.020 inch gap between gates and are interlocked to prevent external ¯elds from penetrating into the trapping region (see Figure 2.5).
- The inject gate is special in that it has two holes in the side. These are used in the fabrication of the photocathode for the introduction of an antimony evaporator and cesium vapor.

Traditionally, the copper gates have been coated with gold for improved electrical conductivity. It is believed that a resistive oxide layer could form on the copper that could then collect unwanted charge, perturbing the electric trapping ¯elds. For several reasons, these gates were not coated with gold:

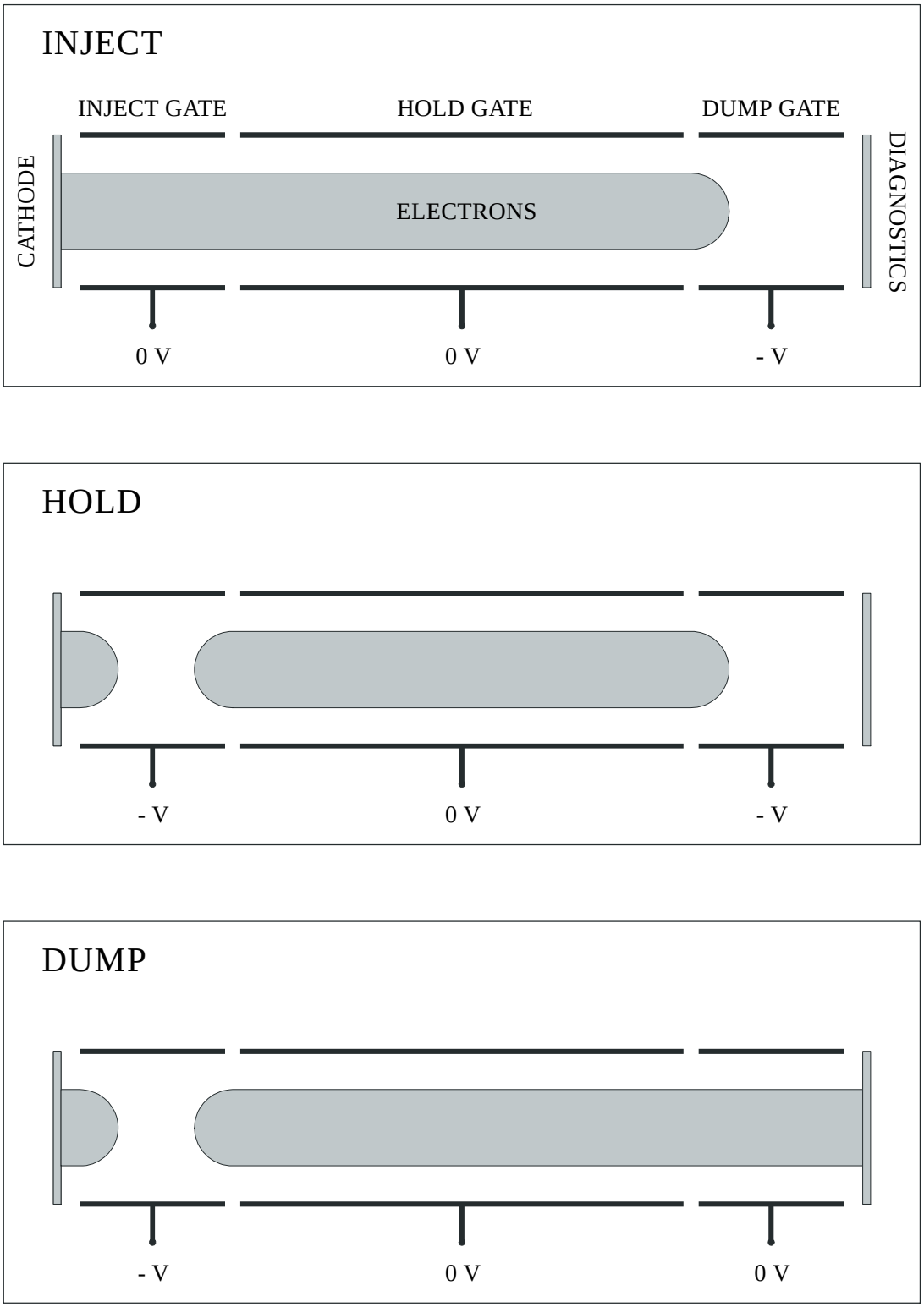

Figure 2.2: The inject-hold-dump experimental cycle.

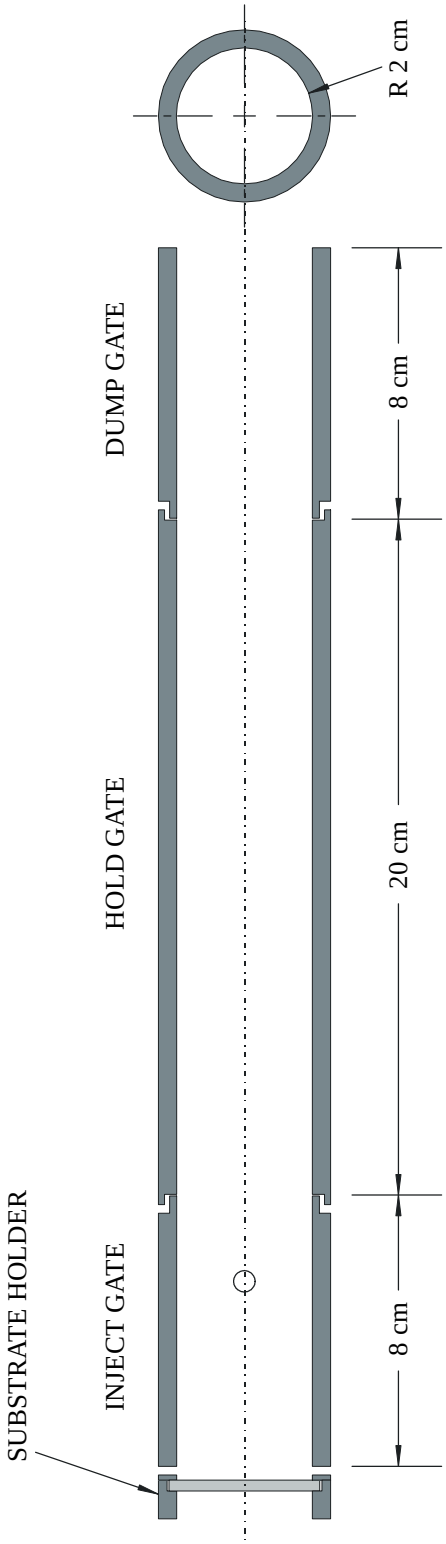

Figure 2.3: Side view of The Photocathode Trap's con¯nement gate region showing the actual layout. Drawn to scale.

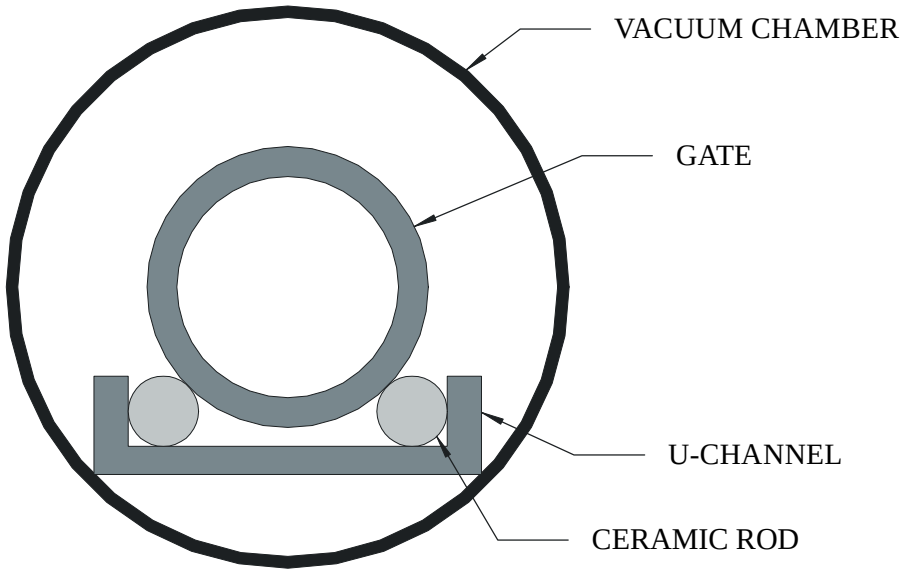

Figure 2.4: The con¯nement gates rest on ceramic rods within a copper U-channel.

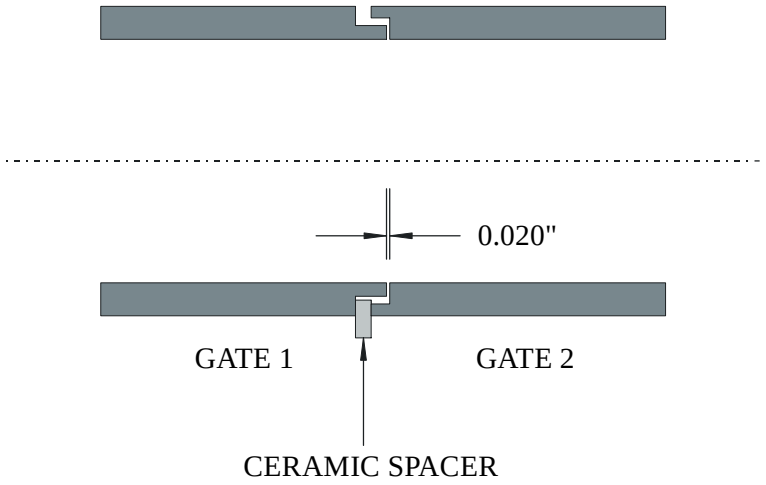

Figure 2.5: The con¯nement gates are interlocked and separated by a ceramic spacer.

- The cesium used in the photocathode's fabrication chemically reacts with gold (ironically also forming a photoemitter).
- The high temperature bake (300 ±C) required to attain ultra high vacuum causes the gold to migrate from the surface of the copper. A nickel strike, which is commonly used to prevent this migration, was not used because of fears that it would perturb the magnetic ¯eld.
- After a photocathode's fabrication and a subsequent exposure to atmosphere, the cesium coated insides react with air and in particular water vapor, requiring a good scrubbing to clean. This would remove any gold coating.

2.1.3 Magnetic Field

The magnetic ¯eld is produced by a superconducting solenoid manufactured by the Kurchatov Institute in Moscow. The wire is Niobium Titanium and superconducts at 10 Kelvin, requiring liquid helium cooling. The magnet is capable of producing a 3 Tesla ¯eld (charged with 130 amps), axially uniform to 0.25 % and azimuthally symmetric to 0.01 % in a 5 cm radius by 60 cm length volume. It also has vertical and horizontal saddle steering coils. The magnet has a hollow 10 inch diameter bore for the insertion of the vacuum chamber housed trap.

2.1.4 Vacuum Chamber

The Photocathode Trap's ultra high vacuum chamber represents a new paradigm for nonneutral plasma traps. Traditionally, vacuum chambers consisted of a horizontal section and a vertical section. The horizontal section housed the trap and that was inserted into the solenoidal ¯eld. The vertical section attached to the end and led down to a large ion pump, which was the main source of pumping (see Figure 2.6). This old design is not e±cient and has a lot of wasted volume, used essentially to get the trap into the uniform magnetic ¯eld region and to distance the ion pump from the solenoid's magnetic ¯eld.

The fabrication of the photocathode mandated a new design (see Figure 2.7). The introduction of antimony and cesium to the substrate required access through the side of the vacuum chamber, which meant it could not ¯t tightly into the magnet's bore. More importantly, because cesium has a tendency to go everywhere and coat everything, I hoped

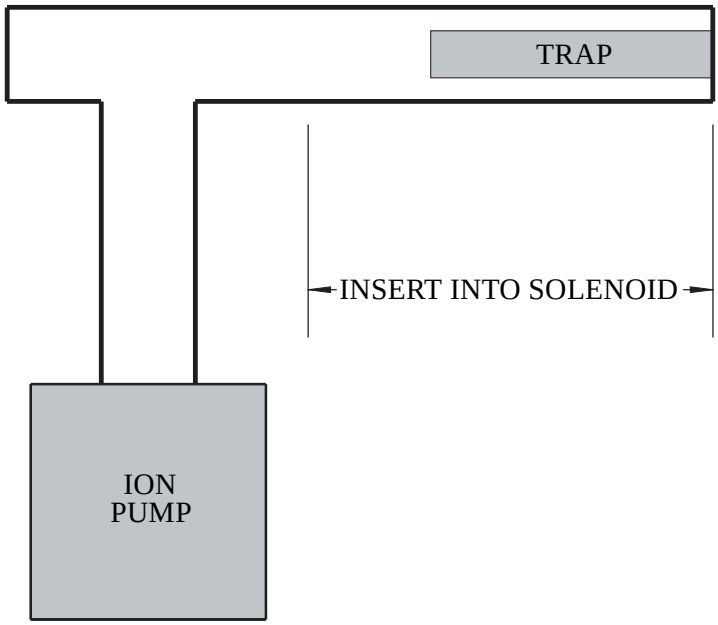

Figure 2.6: The traditional vacuum chamber used for Malmberg-Penning traps.

to minimize the surface area it could stick to. And because I hoped to attain the best possible vacuum, I wanted to eliminate wasted volume.

We had previously experienced problems with cesium migrating to unwanted places during the photocathode's fabrication, in particular into the ion pump. This seriously hindered the performance of the pump, reducing the ultimate achievable vacuum. Therefore, I opted for a two stage pumping process using the combination of a turbo pump and an ion pump. During the initial pump down, bake out, and photocathode fabrication, a turbo pump is used. But, when ready to operate the trap within the solenoid, the turbo pump is valved o® and removed. The trap is then inserted into the magnet's bore. A small homemade titanium ion pump (pumping speed approximately 10 `=s), mounted on the end °ange and using the ambient axial magnetic ¯eld, is then switched on. Using this system, I have been able to achieve vacuums less than 10^{-9} Torr (this measurement comes from the ion pump's power supply, ion gauges will not function in the high ambient magnetic ¯eld).

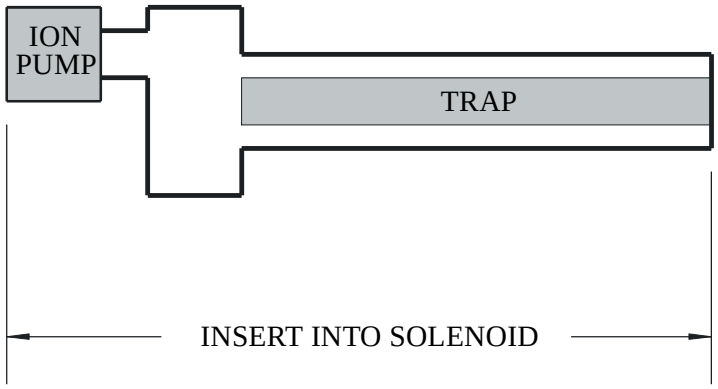

Figure 2.7: The Photocathode Trap's vacuum chamber is e±cient in design. The entire chamber is inserted into the solenoid and the ion pump uses the ambient magnetic ¯eld.

2.2 The Photocathode

Previous Malmberg-Penning traps have used thermionic sources, typically tungsten ¯laments, as electron sources [40]. Electrical current is run through the ¯lament, it heats up, and electrons boil o® the wire. For the smooth injection of an electron column, common wisdom dictates that the electric potential at the cathode match the electric potential in the trap. The electric potential along a ¯lament is given by the ohmic drop. For a circular electron column, the potential is parabolic. To generate the parabolic potential with a ¯lament, it can be wound in a spiral. Thus, cylindrical electron plasmas are typically trapped and need to be manipulated to create multiple columns or hollow ones. Under exceptional conditions, spirals can also be trapped [18].

Thermionic sources have the disadvantage of confounding the electron emission and the potential matching. Electron emission depends on the ¯lament's temperature and therefore on the current through the ¯lament. But the current through the ¯lament also gives the electric potential along the ¯lament, through the ohmic drop. Therefore, both the emission and potential are entangled and are di±cult to reconcile experimentally.

In order to inject more complicated electron pro¯les, a cesium antimonide photocathode was chosen as the electron source. Photocathodes have the advantage of disentangling the emission and potential matching. The electron emission is determined by the light energy illuminating the surface, while potential matching can be applied directly to a conductive substrate.

2.2.1 Cesium Antimonide

Cesium antimonide [41] was one of the ¯rst alkali metal photoemitters discovered. It's stoichiometric composition is Cs_3Sb. It was chosen as the photoemissive material because of its fairly strong quantum yield in the visible (typically 1 to 5 %) and because of its reputed ease of fabrication (only two chemical elements involved) and robustness (can tolerate vacuums of 10^{-6} Torr). This process has proved anything but easy, though. Basically, the fabrication of Cs_3Sb consists of two steps:

1. The evaporation of antimony onto a substrate.
2. The exposure of this antimony coated substrate to cesium vapor, at an elevated temperature to accelerate the chemical reaction.

Both steps must be carried out under vacuum because oxygen and water vapor will attack antimony, cesium, and cesium antimonide.

2.2.2 Fabrication Setup

The integration of a photocathode into a Malmberg-Penning trap presents several challenges (see Figure 2.8). The geometry of the Malmberg-Penning trap is cylindrical, with access to both ends limited. The dump end is occupied by the phosphor screen for imaging. This then dictates the use of a semitransparent transmission photocathode, as opposed to an opaque one. But that now implies that the inject end is dedicated to the introduction of light to illuminate the photocathode. Furthermore, the central volume of the trap cannot be obstructed when trapping electrons. And it all must ¯t inside the magnet's 10 inch bore. This presents two options for the photocathode's fabrication setup:

1. Fabricate the photocathode in a di®erent position, then move it into place.
2. Fabricate the photocathode in place, but move the antimony evaporator.

The ¯rst option is awkward given the geometry and involves precisely moving the photocathode substrate. The second option was chosen and the antimony evaporator was mounted on a bellows and given side access through the inject gate (see Figure 2.9).

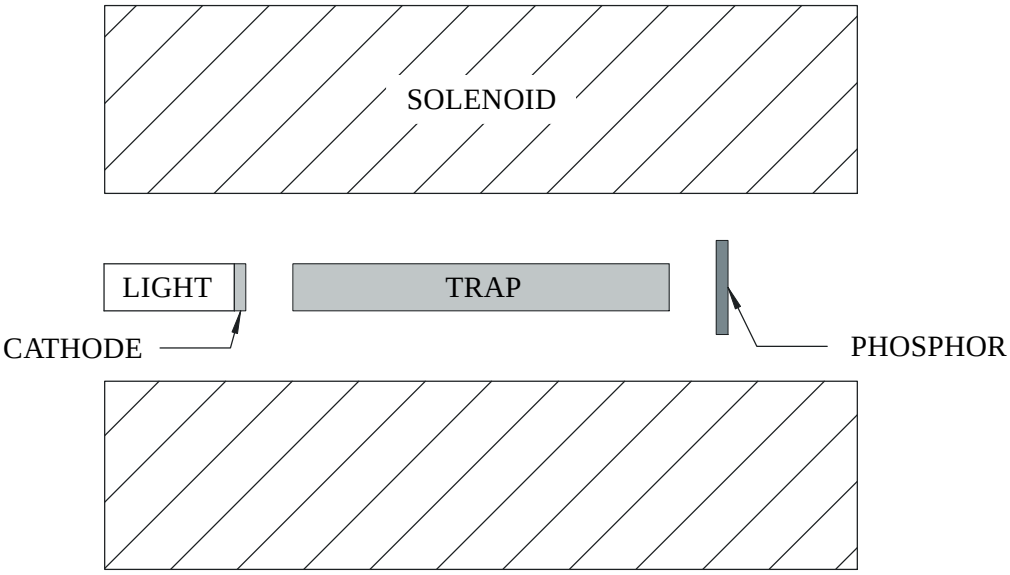

Figure 2.8: The photocathode fabrication constraints.

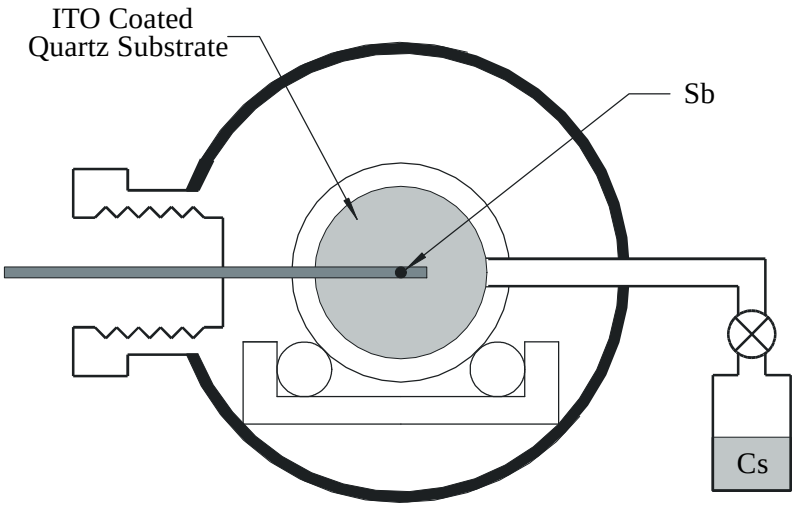

Figure 2.9: The experimental setup for the photocathode's fabrication.

2.2.3 Recipe

The recipe for fabricating a cesium antimonide photocathode is presented here. The included details are speci¯c to The Photocathode Trap.

Supplies:

- 1 bead of antimony (supplied by Aldrich Chemical Company) melted onto nichrome wire of 0.5 mm diameter. I fabricated this by melting the antimony onto the nichrome in a low vacuum chamber [42]. Cesium will react with the antimony evaporator, but it can be reused if it is cleaned.
- 1 gram ampoule of cesium (supplied by Aldrich Chemical Company). The ampoule is loaded into a thin-walled stainless steel tube and attached to the main chamber via a needle valve. The tube is ¯rst pumped out, next the ampoule is broken by squeezing the tube with channel locks, then the cesium tube is pumped out before the valve is closed. Typically, this is enough cesium for three runs.
- 1 unleaded glass or quartz substrate, coated with indium tin oxide (a transparent conductor). The glass disks were manufactured by the LBNL optics shop and the coating was done by Metavac to better than 20 -=2.

Procedure:

1. Clean all parts to ultra high vacuum standards. The photocathode substrate is cleaned with soapy water, trichloroethane, ethyl alcohol, and ¯nally distilled water. Feedthrus can be cleaned with hydrogen peroxide.
2. Within the vacuum chamber, position the antimony evaporator in front of the glass substrate, but at some distance away. This will represent a trade o®, as you would like the evaporator as far away as possible for a uniform deposition, but will be constrained by your trap. For this system, the evaporator was mounted approximately 5.5 cm away from the 4.0 cm diameter substrate.
3. Pump down vacuum chamber with the turbo pump to less than 10^{-6} Torr.
4. Antimony deposition:

(a) Shine white light (a slide projector works well) from the phosphor screen end of the chamber through the substrate and monitor the light transmission with a CdS photocell.

(b) Slowly (over 20 minutes) warm up the antimony evaporator, keeping the pressure below 10^{-5} Torr and monitor the light transmission (LabView routine \Sb deposition GPIB.vi"). Typically, evaporation will begin around 3 amps.

(c) When the light transmission drops to between 60 and 80 % of the initial value, cease antimony evaporation. Once evaporation starts, this typically takes 20 seconds. The layer will be noticeably darker and grey, but should appear uniform.

(d) Withdraw the antimony evaporator from the trap.

5. Bake out the vacuum chamber, typically to at least 200 ±C (usually 300 ±C), and the turbo pump for 1 week. The turbo pump will require water cooling during its bake out. The pressure should be monitored for signs of leaks (LabView routine \pressure chart.vi"). At the end of the bake and while the chamber is still hot, the pressure should be below 10^{-6} Torr.

6. Cesium release:

(a) Adjust the chamber temperatures such that the substrate is between 120 and 140 ±C AND that regions where cesium is not welcomed (high voltage feedthru, ion gauge, ion pump) are at least 300 ±C to prevent the condensation of cesium there. Excess cesium on the high voltage insulator will make it di±cult to maintain the high voltage necessary for imaging. Excess cesium on the ion gauge will perturb the pressure reading. The turbo pump should still be baking.

(b) Set up to monitor photocurrent (LabView routine \photocurrent.vi"), ¯rst with a slide projector, then with a green laser of known power. Knowing the laser power and the expected quantum e±ciency of at least 1 %, you can calculate the expected photocurrent. I used a 0.75 mW green HeNe laser centered at 543 nm. For a 1 % quantum e±ciency and ignoring transmission losses through the viewport, this should produce 3 microamps of photocurrent.

(c) Apply at least -10 volts to the substrate, with the trap gates and chamber grounded. This voltage will depend on the trap geometry and expected photocurrents, and you should be aware of the space charge limitations. Monitor

the photocurrent with an ammeter between the power supply and the substrate (it should be sensitive to at least 0.1 microamps). There will be dark current (typically less than 1 microamp), so the photocurrent is measured by reading the current with light and subtracting the current without.

(d) While monitoring the photocurrent, open the cesium valve and then slowly (over 10 minutes) warm the cesium chamber to 200 ±C. Be careful not to introduce too much cesium into the chamber, as cesium is di±cult to pump out and this will hurt the ultimate vacuum.

(e) Once photocurrent levels out near the expected level (typically 5 microamps for my system with the 0.75 mW green laser), close the cesium valve and allow the vacuum to recover. Be careful, though. As the cesium reacts with the antimony, di®erent compounds are formed and this will correspond to a leveling o® and perhaps even decrease of the photoemission. These photocurrents will be more than an order of magnitude below the expected ¯nal photocurrent.

7. Cool ¯rst noncritical chamber parts to room temperature, then cool the critical parts, such as the high voltage feedthru and the turbo pump. Typically, the photocurrent will rise during the cool down, sometimes by as much as 100 %.

8. Once the chamber has cooled to room temperature, make a photocurrent map of the substrate. First, determine the optimal cathode voltage to overcome space charge limitations. Then, with this voltage applied to the cathode, map out the photoemission with the laser. Typically, you should ¯nd quantum e±ciencies of 1 to 5 % (approximately 3 to 15 microamps for my system with the 0.75 mW green laser) with variations across the cathode on the order of 10 % of the peak value. White light through the photocathode should appear noticeably red. If it appears yellow, then the chemical reaction was not carried out to completion.

Revitalization Procedure:

If the photocathode fabrication was terminated too early, or if the photocathode has weakened during use, then it may be possible to revive it. Essentially, the procedure is to release more cesium as described above. Note that this will only work if the reason for a weak photocathode is not enough cesium. If the reason is that the cesium antimonide has been chemically attacked, then the whole fabrication must be begun anew.

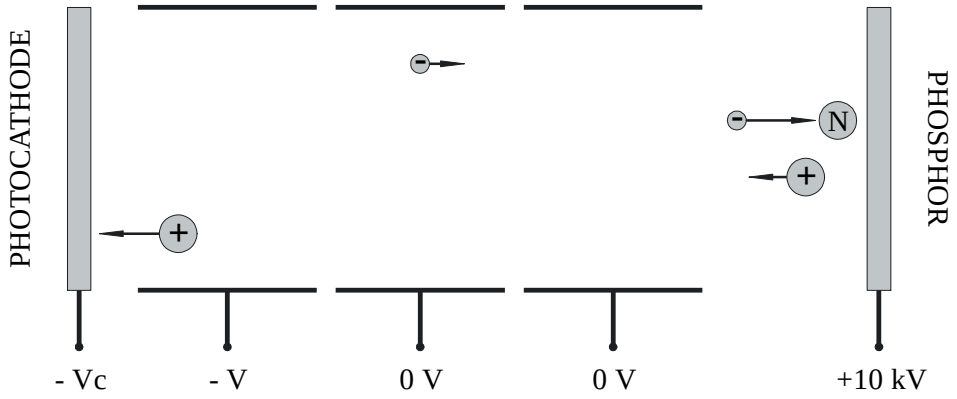

Figure 2.10: Ions formed in the vicinity of the phosphor are unintentionally accelerated into the photocathode, thereby damaging it.

2.2.4 Lifetime

A serious challenge to using a photocathode in a Malmberg-Penning trap has been keeping it alive. During the operation of a photocathode, it has been observed that the quantum e±ciency decreases, unfortunately often dramatically. I believe that one cause of this e®ect is due to ion bombardment (see Figure 2.10). Ions are generated in the vicinity of the phosphor screen, probably by electrons being accelerated towards it. These ions are created at electric potentials of at least 10 kilovolts and are naturally accelerated away from the phosphor, along the magnetic ¯eld lines, and right into the photocathode, where they break up the cesium antimonide. There are several ways to reduce this problem:

- Operate with the lowest possible vacuum to reduce the collisional ionization.
- Minimize the charge being dumped onto the phosphor. For instance, in the course of focusing the light source or steering the magnetic ¯eld, it is useful to accelerate electrons o® the cathode and directly onto the phosphor. As a warning, do not stream electrons onto the phosphor unnecessarily, but rather chop the beam instead.
- Minimize the time that high voltage is being applied to the phosphor and make the most of the run time.

2.2.5 Light Source

The light source used to deliver an image to the photocathode was designed in collaboration with undergraduate Lluvia Zuñiga (see Figure 2.11). The simple goal of the

light source is to deliver as much light as possible to the photocathode. There were other design constraints:

- The light is provided by a halogen slide projector lamp, type EXW. The diameter of this bulb is approximately 3 cm and this will limit the size of the uniform light beam that can be condensed.
- The slides are produced using an ink jet printer. The printer has a ¯nite resolution of 360 dpi. This will then limit the resolution of the image produced. This resolution is comparable to the resolution of the CCD imaging system (see Section 2.3.1).
- The photocathode is approximately 8 cm from the viewport, because of the vacuum chamber design. Therefore, any optics will be at least this distance away from the image plane.

We determined that the optical system that best achieved the goal of producing a bright, uniform image under these constraints had a magni¯cation of 1. The system is essentially that of a Kodak slide projector, from which the heat glass and condenser were scavenged. The objective is two plano-convex lenses (each has a focal length of 125 mm) placed back to back. It represents a cost e®ective means for achieving decent image quality. An aperture with a diameter of 1 inch is also used to reduce aberration.

Because the light bulb can get very hot and heat the inner bore of the magnet, a simple air cooling system made out of a blow dryer is used.

This light system, with the bulb running at 40 volts (AC), delivers to the photocathode a luminous °ux of approximately 2000 lux, equivalent to approximately 0.30 $mW=cm^2$ of white light. Running at 80 volts delivers approximately twice as much luminous °ux.

2.2.6 Performance

The cesium antimonide photocathode, in conjunction with the above light source, has performed comparably to the thermionic sources. Typically, electron systems with densities of $3 £ 10^7 cm^{-3}$ and temperatures of 3 eV are injected, corresponding to Debye lengths of approximately 0.2 cm. These parameters do depend on the intensity of the light source and the cathode voltage, though.

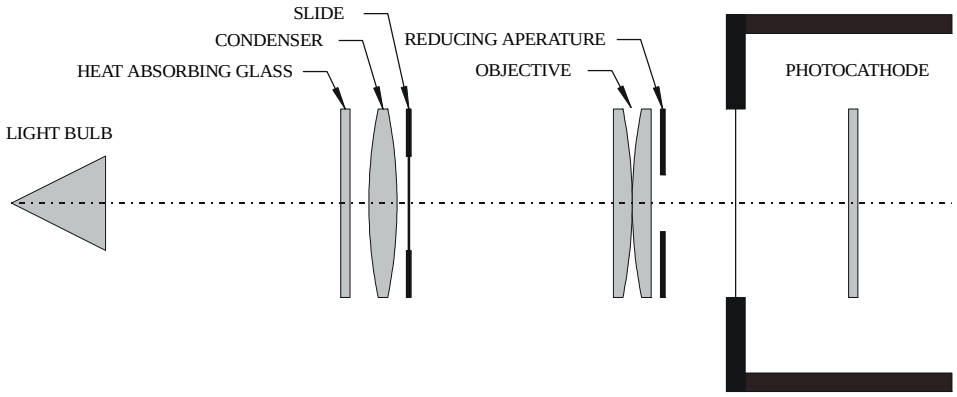

Figure 2.11: The light source for delivering an image to the photocathode.

2.2.7 Examples

The following examples demonstrate the advantage of the photocathode over previous thermionic sources for injecting complicated electron pro¯les. Remember that a spiral ¯lament naturally injects a column of electrons and that the column must be manipulated to generate other pro¯les.

- The Diocotron Instability: (see Figure 2.12) The Diocotron Instability is analogous to the Kelvin-Helmholtz Instability in °uid shear layers. The radius and thickness of the ring determine how many vortices it will evolve into. This experiment was originally performed by Peurrung and Fajans [12] using a thermionic source. In that experiment, an electron column was initially injected, then the dump gate was only partly lowered, allowing the central electrons to escape. The dump gate was then raised back up, trapping the remaining ring of electrons. Here, a ring of light illuminated the photocathode and a hollow column of electrons was initially injected.

- The Pairing Instability: (see Figure 2.13) The Pairing Instability occurs when two vortices are closer than a critical separation distance and then merge. If the vortices are separated by more than the critical distance, then they will orbit about the trap center and not merge. This experiment was originally performed by Fine, Driscoll, Malmberg, and Mitchell [13, 36] using a thermionic source and a trap with several hold gates. In that experiment, an electron column was initially trapped. Then, one of the hold gates was raised, cutting the column into two. The two columns were then de-phased, the hold gate was lowered, and the two columns expanded into the

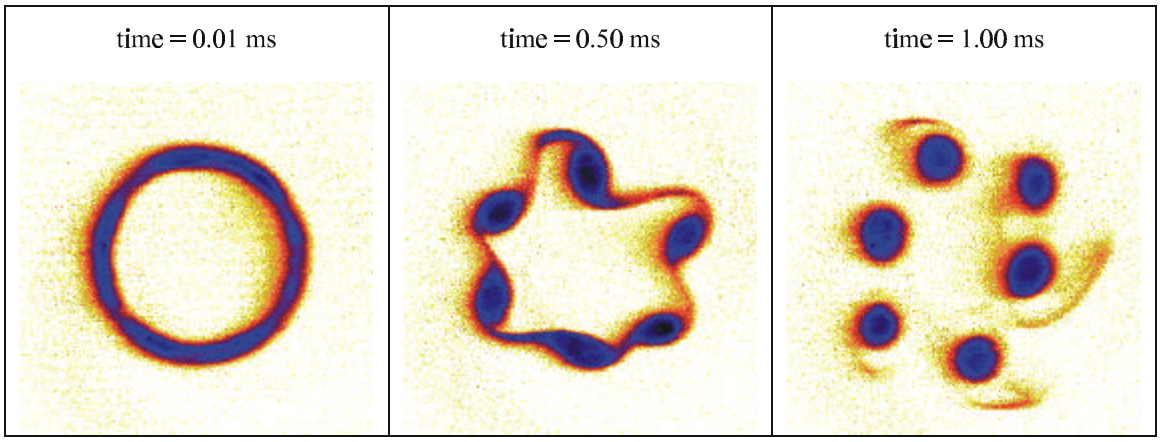

Figure 2.12: The Diocotron Instability.

total length of the hold gate, thereby creating two separate columns. Here, two circles of light illuminated the photocathode and two columns of electrons were initially injected.

- 19 Vortices: (see Figure 2.14) Experimentally studying the stability of many-vortex patterns is the emphasis of this thesis and the subject of Chapter 4. Here is an example of a pattern of 19 vortices that is stable for over 100 bulk rotations. This pattern would be extremely difficult to inject without a photocathode.
- Go Bears!: (see Figure 2.15) Injecting a "C" for The University of California at Berkeley that then evolves as a partial ring, breaking into vortices.
- Anchors Away!: (see Figure 2.16) Demonstrating the capabilities of the photocathode to inject complicated profiles. For The Office of Naval Research, our sponsors.
- The Fajans Instability: (see Figure 2.17) Everyone can have an instability with the photocathode. Here, the image of my research advisor is definitely unstable.

2.3 Diagnostics

The diagnostics available for The Photocathode Trap are all destructive. The electrons are dumped from the trap and to continue experiments, new electrons need to

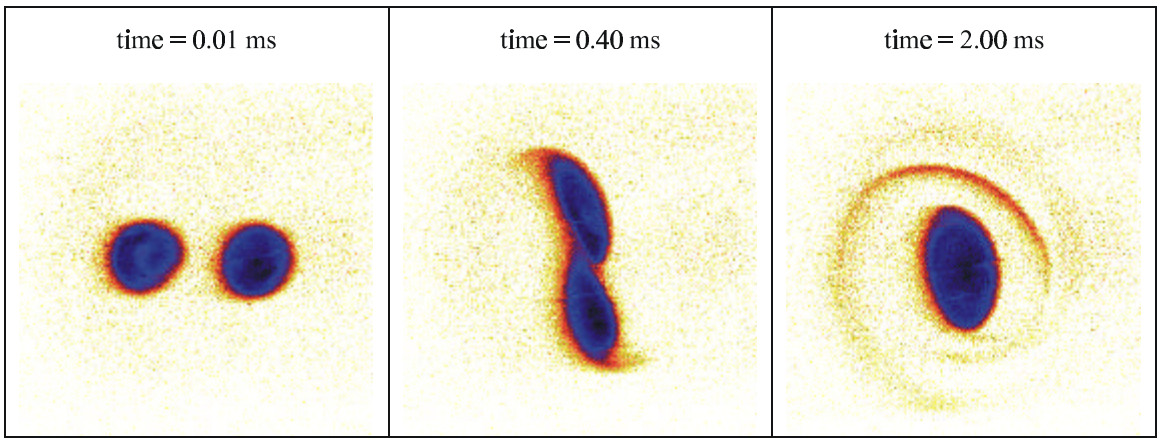

Figure 2.13: The Pairing Instability.

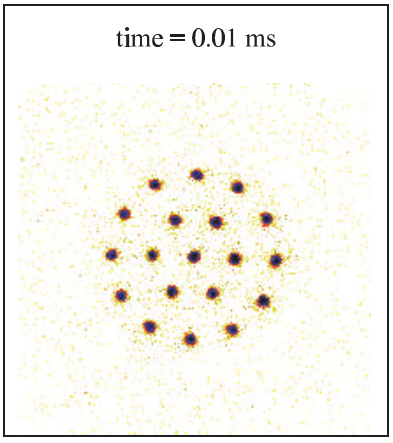

Figure 2.14: A stable 19 vortex pattern.

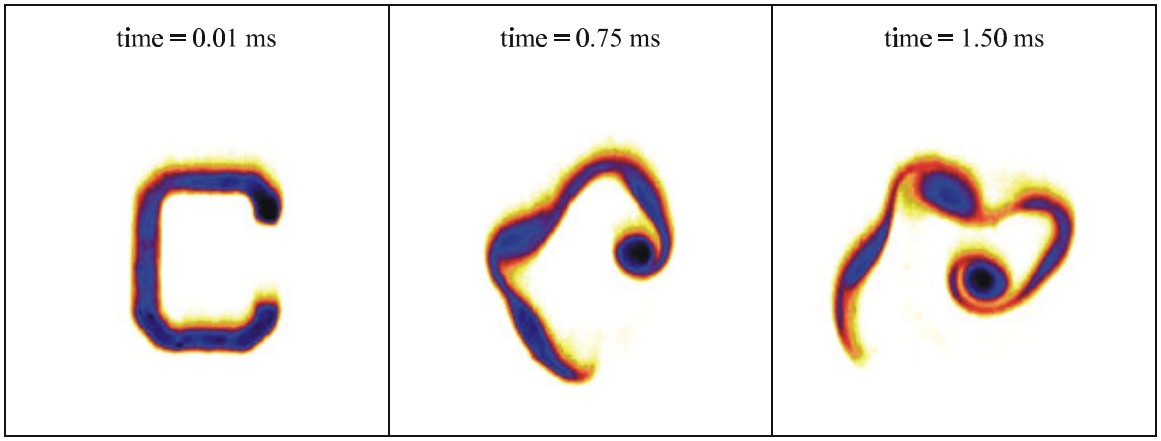

Figure 2.15: Go Bears!

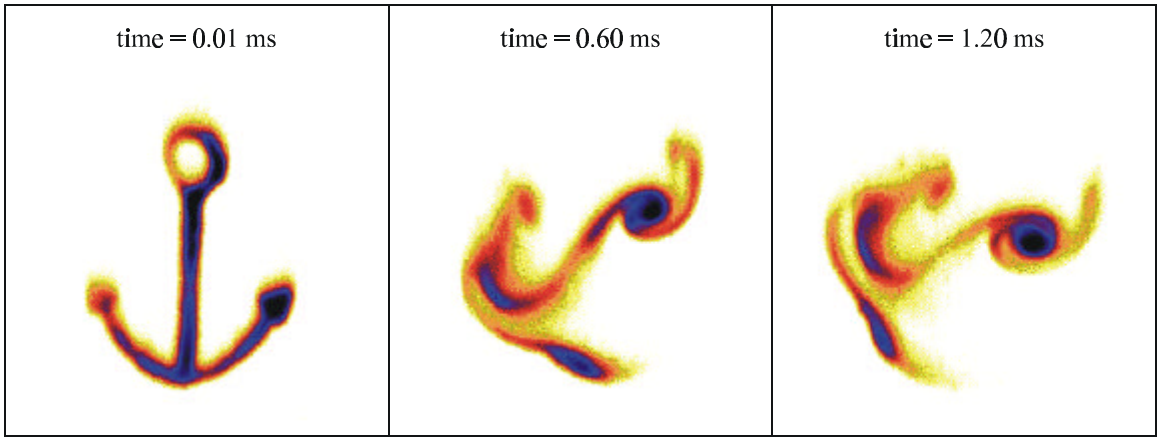

Figure 2.16: Anchors Away!

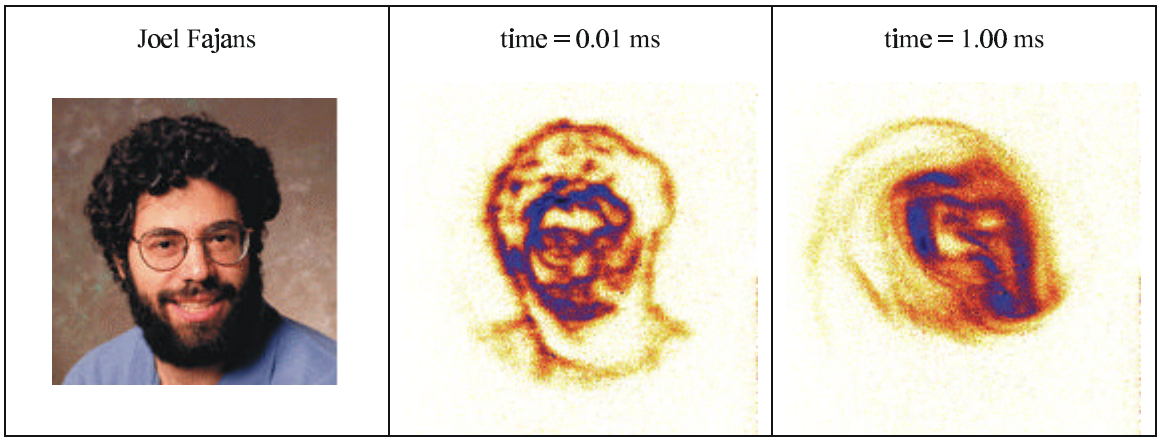

Figure 2.17: The Fajans Instability.

be injected. Note that \sectored gates" that are commonly installed in other Malmberg-Penning traps are not here, but they could easily be if the demand arose.

2.3.1 Imaging System

The main diagnostic for the Photocathode Trap is an imaging system using a phosphor screen (manufactured by Grant Scienti¯c) [43, 44] and a liquid nitrogen cooled CCD camera (manufactured by Princeton Instruments). The electrons are imaged by grounding the dump gate. They stream along the magnetic ¯eld lines and are accelerated to at least 10 kV, into the phosphor screen. They then produce light which is detected by a CCD camera looking through a viewport at the phosphor screen.

During the acceleration of the electrons, you would like to minimize image distorting radial electrical ¯elds. The radial electrical ¯elds cause azimuthal E £ B smearing. Traditionally, a stack of rings linked by high voltage resistors has been used to force an axial electrical ¯eld. But, high voltage ultra high vacuum compatible resistors have been di±cult to acquire. They also limit the bake out temperature of the chamber and may outgas. Regardless, the whole construction is unnecessary. Kevin Fine has suggested a way in which the acceleration rings can be removed (see Figure 2.18). The phosphor screen is held by a disk that is at least twice the diameter of the inner gate diameter. This phosphor and holder is mounted a distance away from the end gate equal to the larger diameter. Another disk of the same diameter is mounted just behind the dump gate and grounded. The whole

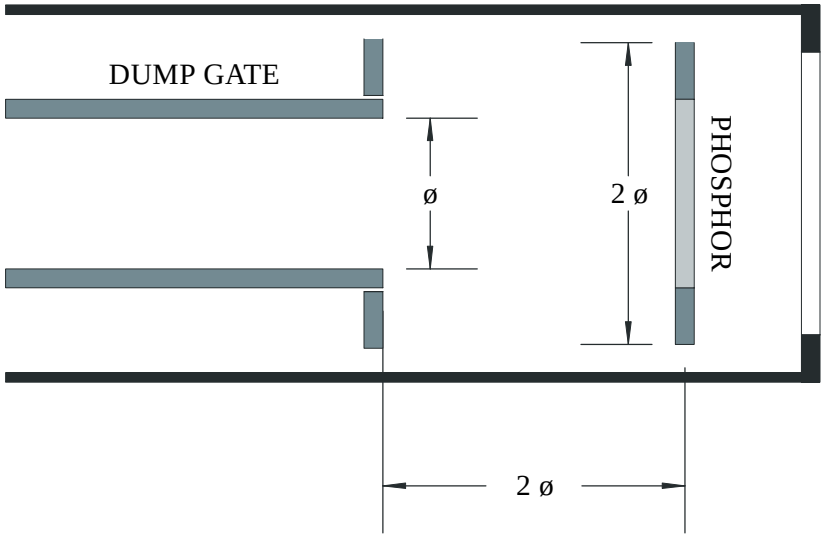

Figure 2.18: The imaging system for The Photocathode Trap.

region is contained within a cylinder of a diameter just slightly larger, and is also grounded. This setup has the e®ect of pulling radial electric ¯eld components out towards the wall. In the central region, where the electrons will be accelerated, the ¯eld is essentially axial.

There is a problem of the light being used to illuminate the photocathode interfering with the image from the phosphor. This problem is reduced in several ways:

1. The phosphor is coated with an aluminum layer to reduce light transmission.
2. The phosphor used is P43 with a wavelength response between 540 and 550 nm coupled with a ¯lter (manufactured by Barr Associates) on the CCD camera tuned to pass a central wavelength of 545 nm and a band pass of 22 nm.
3. The phosphor's decay time is about 3 ms, so the CCD camera's shutter is opened for just enough time to catch this image and no more, thereby reducing the noise. The pneumatic shutter is mechanically limited to a 10 ms open time and a delay of 10 ms.
4. The CCD camera's imaging software can subtract a background image.

By utilizing the above techniques, the background has been reduced to 1 unit of brightness, compared to 100 units for the image of an electron system with a density of $1 £ 10^7\,cm^{-3}$, running with the phosphor at 14 kV.

The resolution of this imaging system is approximately 105 pixels=cm, but does depend on the camera's placement.

2.3.2 Total Charge

A more basic diagnostic determines the total trapped charge. The phosphor is used as a charge collector and the electrons are dumped onto it. Knowing the capacitance to ground allows you to calculate the total charge. The capacitance of The Photocathode Trap's phosphor to ground is typically 350 pf.

As a warning, this diagnostic has proven unreliable and therefore can give incorrect total charge measurements. There appears to be a problem with the phosphor screens and in particular with making electrical contact with either the aluminum layer or the indium tin oxide layer. Not all phosphor screens exhibited this problem even though they were all ordered under identical manufacturing speci¯cations.

2.3.3 Temperature

The trapped electron system's axial temperature is measured by slowly ramping the dump gate and allowing the hottest electrons to escape ¯rst [45]. If the system is Maxwellian, then in e®ect the tail of the distribution is being sampled and the temperature can be determined. The electrons need to be dumped slower than the bounce time, but faster than the collision time (so that they do not re-thermalize) and any instability time (such as the hollow ring instability).

Note that for this procedure, a Maxwellian distribution is assumed. It is clear that for a majority of the experiments considered here, with extremely fast inject times, that the system has not yet had a chance to come into thermal equilibrium and that therefore this procedure is not really applicable.

2.3.4 Axial Pro¯le Calculation

Given the radial pro¯le of the electron system and its temperature, and assuming that the system is in thermal equilibrium and is azimuthally symmetric, then the axial pro¯le can be calculated via computer [46, 47]. A computer program calculates the electron density determined by the Maxwell-Boltzmann distribution, then calculates the electric potentials by the Poisson equation given by this distribution, then iterates back to the

Maxwell-Boltzmann equation to recalculate the densities, and so forth. In such a way, the density distribution relaxes to the physically correct answer.

This technique is useful in checking the various density measurements. The method of measuring the diocotron period and then calculating the density is susceptible to ¯nite length e®ects. The method of dumping charge is also dependent on the length of the electron system. Therefore, the axial pro¯le calculation can help determine what the length actually is for a trapped system.

Chapter 3

The Equipotential Cathode

The operation of cathodes is a bit of an unexplored mystery in the ¯eld of Non-neutral Plasma Physics. It seems that we experimentalists are simply happy when they do work, we don't ask too many questions, and we just forge ahead with the planned experiments. This mystery applies not just to the photocathode, but to the traditional tungsten ¯lament as well.

3.1 Electron Injection

It is commonly believed that to inject an electron system, the electric potential at the cathode needs to closely match the electric potential in the trap where the electron is going [40]. If the cathode potential were too high, the electron would enter the trap with excess energy and this would translate into a higher temperature. If the cathode potential were too low, the electron would be re°ected by the space charge in the trap.

For illustration, consider the simple 1D model of the injection phase of electrons into the trap (see Figure 3.1). During the inject phase, the inject and hold gates are grounded and the dump gate is at some negative electric potential. Let us assume that electrons have already ¯lled the trap and that therefore their space charge has contributed to the potential energy in the trap. For an electron to enter the trap, it must be emitted from the cathode at a potential close to that in the trap. The electron's initial potential energy can be slightly less, as long as it has enough kinetic energy to overcome the space charge potential barrier. If the initial potential energy is too high, this will correspond to the electron's kinetic energy increasing in the trap, and therefore its temperature increasing.

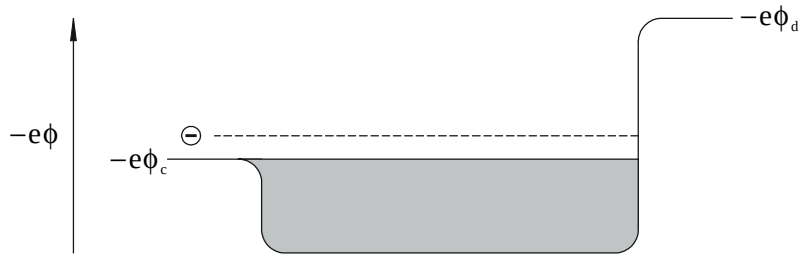

Figure 3.1: 1D steady-state inject model.

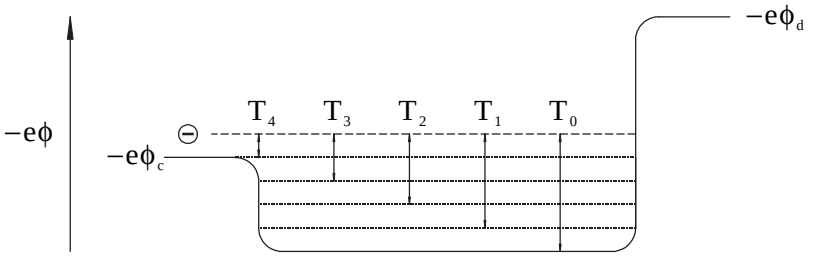

Figure 3.2: 1D trapping model.

As a final note on this ideal model, an electron that does enter the trap should travel to the dump gate barrier, reflect, and then travel back out of the trap.

Now let us examine how the electrons got into the trapping region in the first place (see Figure 3.2). We shall see that the devil is indeed in the details. Again, let the inject and hold gates be grounded and the dump gate be at some negative potential. Set the cathode voltage at some specified value. Initially, there are no electrons in the trap and therefore no space charge. Electrons will begin to travel from the cathode into the trap, and because there is initially no space charge in the trap, the electrons will have a kinetic energy corresponding to T_0. As they fill the trap, the space charge potential begins to build, and newly entering electrons will acquire less kinetic energy (for instance, T_1 through T_4, when the trap is full). As the velocity of the newly entering electrons in the trap decreases, the density increases by the conservation of $j = nev$, again helping to build the space charge potential. Note that electrons entering the trap are reflected off the dump gate and should exit the trap. The only trapping occurs when the inject gate barrier is raised. All is still well.

All would still be well if it were not for the fact that experiments do not behave this way. First, spiral tungsten filaments, or any shaped filament for that matter, should

not inject circular columns. They should inject spirals, or whatever the ¯lament's shape is. Secondly, an equipotential cathode should not work, but I have megabytes of pictures that say that it does. There appears to be more to the story.

3.2 Spiral Filaments

Spiral ¯laments have commonly been used as electron sources because of their ability to inject circular columns. Theoretically, the ohmic drop along the ¯lament can be made to match the potential of a circular column of given radius and electron density by tuning the bias of the ¯lament and the drop across the ¯lament. By the above model, though, a spiral should always be injected. Experimentally, it is observed that for extremely short inject times, on the order of the electron bounce time in the trap, spirals are indeed injected. But under normal operation conditions, where much longer inject times have traditionally been used, circular columns are injected. This strongly implies that electrons are being trapped in the trapping region even while the inject gate is grounded. There are several possible mechanisms for how this could happen:

- An electron travelling in the trapping region experiences a collision that lowers its energy (see Figure 3.3). By the time it re°ects o® the dump gate and returns to the cathode, its energy has been lowered to a level where it can no longer exit over the cathode potential. The cathode acts as a barrier and the electron is now trapped. This possibility predicts a dependence on electron and background gas collision rates.

- An electron travelling in the trapping region has its radial position changed, either by a collision or by E £ B motion (see Figure 3.4). It changes to such a radial position that when it returns to the cathode, the cathode potential energy at the new radius is higher than at the original. This will act as a potential barrier and the electron will then be trapped. Note that this possibility exists for only non-equipotential cathodes.

- Electrons re°ecting o® the dump gate will encounter electrons emitting from the cathode. This could lead to streaming instabilities.

Another phenomena has been observed with a spiral ¯lament that was ¯rst noticed here with an equipotential photocathode. This is the dependence of the electron system's pro¯le on the inject time and the observation of hollow pro¯le injections, implying the

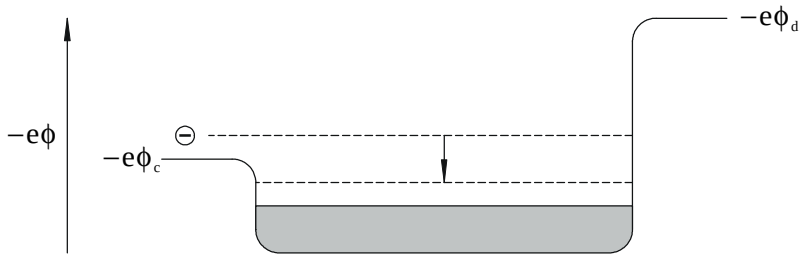

Figure 3.3: Collisional trapping model.

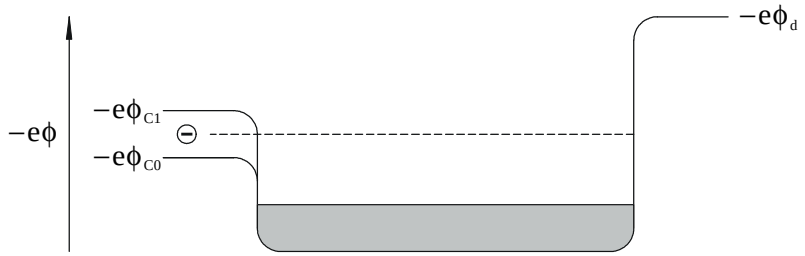

Figure 3.4: Radial position trapping model.

suppression of electron injection at the center of the cathode. This is again accountable by the trapping of electrons during the injection phase. More will be said about it in the next section.

3.3 The Equipotential Photocathode

That an equipotential photocathode has worked so well, albeit in a limited capacity, has been a surprise to most in the ¯eld [48]. Originally, an option to control the electric potential across the surface of the cathode was even developed (see Appendix C). Kreisel and Driscoll [49] have predicted that an equipotential cathode should inject a hollow electron pro¯le. In their model, they assume a Maxwellian distribution for the injected electrons, implying that their system is in thermal equilibrium. Though that may be true for long inject times of many collisional times, that is not true for fast injects where the system has not had time to thermalize.

For a photocathode, there are essentially three parameters that control the injection of the electrons:

- light source brightness

- inject time
- cathode voltage

Experimentally, the electron systems are barely within imaging capability as it is, so in order to inject the densest systems, the brightest possible light source is used. This leaves the inject time and the cathode voltage as the two parameters to tweak.

3.3.1 The E®ect of Inject Time

A strong dependence of the electron pro¯le on the inject time is observed. The longer the inject time, the greater the distortion of the pro¯le. Consider the example of injecting an \anchor" pro¯le (Figure 3.5). The cathode was ¯xed at -3.2 volts and the inject time was varied. The electron system was held for less than 0.01 ms before imaging, corresponding to a virtually immediate dump. Notice the presence of a di®use background of electrons that increases in size as the inject time becomes longer. No light is striking the photocathode where these electrons are; therefore, these electrons must have been originally injected where the anchor is, become trapped during the injection phase, and then moved in position to form the background cloud. Also note that an inject time of 0.01 ms gives a nice pro¯le and that at 0.10 ms the distortion is obvious and the formation of the background cloud is well under way.

One mechanism that accounts for this trapping during injection is collisions with the background gas, as was discussed earlier (see Figure 3.3). An electron that has undergone a collision could become trapped. For a system with an electron density of $1 £ 10^7$ cm^{-3}, an electron temperature of 1 eV, and a background gas pressure of 10^{-8} Torr, the electron-electron collision time is on the order of 1 ms and the electron-neutral collision time is on the order of several milliseconds, depending on the residual gas. If it is nitrogen, then the collision time is closer to 10 ms, but if it is cesium, as it may very well be, then it is closer to 1 ms. A di®use electron cloud will perhaps also form on this time scale. Unfortunately, a residual gas analyzer could not function in the large magnetic ¯eld. So, we could not determine the residual gas composition under operating conditions.

To test the above model, the dependence of the electron pro¯le on the background gas pressure at a given inject time should be studied. The prediction is that for higher background pressures, the injected pro¯le should become more distorted. Unfortunately, I do not have good control over the pressure in my experiment to test this. Clearly though,

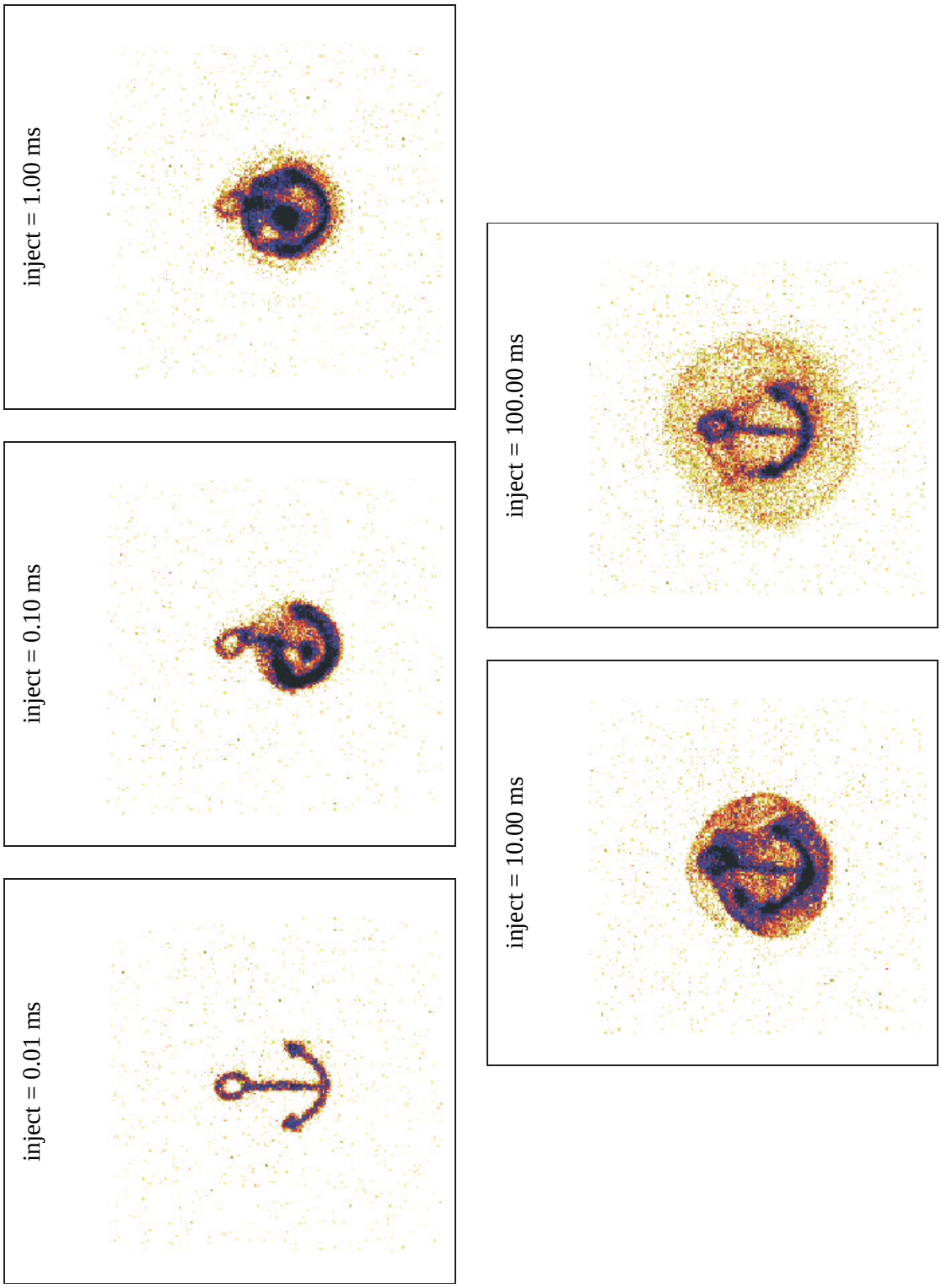

Figure 3.5: Inject time phenomena. For a ¯xed cathode voltage, the inject time is varied and the injected electron pro¯le is imaged. An \anchor" slide is used to demonstrate the distortion of the pro¯le.

the lesson here is that in order to inject distortion free pro¯les, a fast inject time must be used.

3.3.2 The E®ect of Cathode Voltage

There is also a strong dependence of the electron pro¯le on the cathode voltage. When doing the experiments on 2D vortex patterns (see Chapter 4), I would have to tune the cathode voltage to get the most uniform injection. If the voltage was too low, then the pro¯le's density would be too weak. If the voltage was too high, then again the pro¯le's density would be too weak, or sometimes hollow. There was clearly an optimal cathode voltage for a given pattern.

Here I present data for injecting an electron column of radius 0.50 cm and varying the inject time at cathode voltages of -5, -10, and -20 volts. For reference, the central voltage of the electron column was calculated to be approximately -1 volt, but did depend on the electron pro¯le.

- cathode = -5 volts: (see Figure 3.6) For an inject of 0.01 ms, the initial pro¯le is weak, but does have a peak in the center. For longer inject times, the central emission is suppressed and rings are injected. For 100.00 ms, a large di®use electron background is observed with emission only at the column's outer edge.

- cathode = -10 volts: (see Figure 3.7) For an inject of 0.01 ms, the initial pro¯le is stronger than compared to a cathode voltage of -5 volts. Again, the pro¯le becomes hollow with increasing the inject time. An extremely interesting pattern is observed for an inject of 100.00 ms. Here, the outer edge of the column is again observed, but so are 6 vortices symmetrically arranged about the ring, perhaps remnants from a diocotron-unstable ring formed earlier during the inject phase. Also evident are \tendrils" of electrons extending from 3 of these vortices to the ring and 2 \hollow" vortices.

- cathode = -20 volts: (see Figure 3.8) Because of the larger cathode voltage, it now takes longer for the space charge to build up and suppress the cathode's central emission. At an inject of 0.10 ms, the optimal electron pro¯le is observed for this experiment. It is extremely uniform.

A general feature to note is that as the inject time increases, the hollowness of the pro¯le also increases. What is happening is that as electrons are ¯lling the trap and the space charge in the trap is suppressing emission from the cathode. The space charge produces a potential that is most negative at the trap's center, so that the center of the cathode is the ¯rst to experience suppressed emission while the outer radii of the cathode are still emitting. In this way, a ring of electrons gets injected. When the density of this ring becomes large enough, it can be observed to go unstable via the diocotron instability (see 1.00 ms for Figure 3.8).

In summary, it was found that to inject the column with a radius of 0.50 cm, a cathode voltage of -20 volts and an inject of 0.10 ms produced the best pro¯le. The temperature of this system was measured to be 3 eV by the method described in Section 2.3.3, but again the caveat is that the system is really not in thermal equilibrium. The Debye length was calculated to be on the order of the column's radius.

3.4 Summary

I was able to demonstrate that an equipotential cathode could inject a uniform pro¯le in at least some regime. But, there remains an open question as to whether an equipotential cathode can inject a column of many Debye lengths in radius. The belief is that if the electron column has a radial potential drop of many volts, then there may be a correspondingly large electron temperature distribution. Further work needs to be done to answer this question.

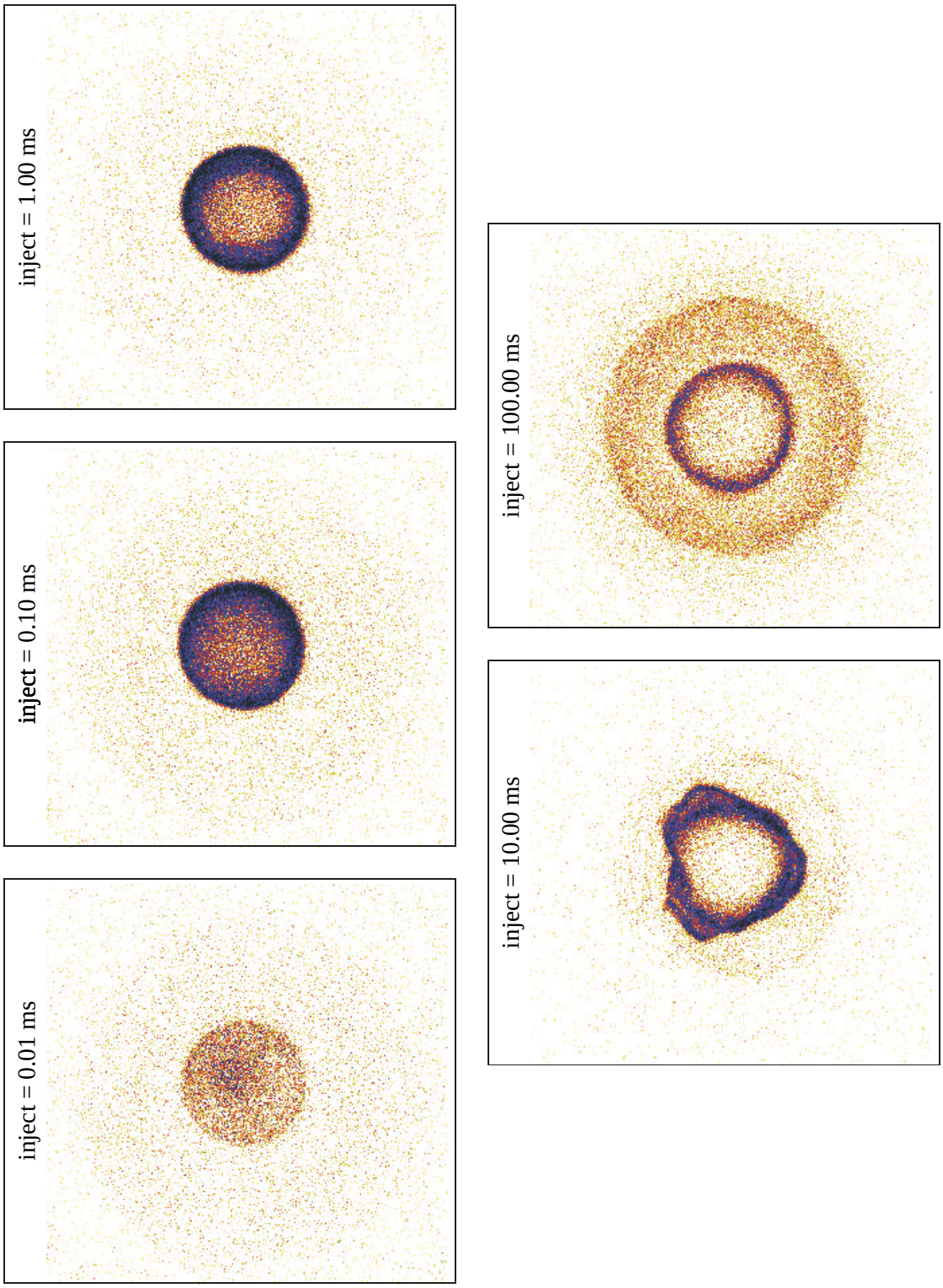

Figure 3.6: Electron Pro¯le vs Inject Time, -5 V Cathode.

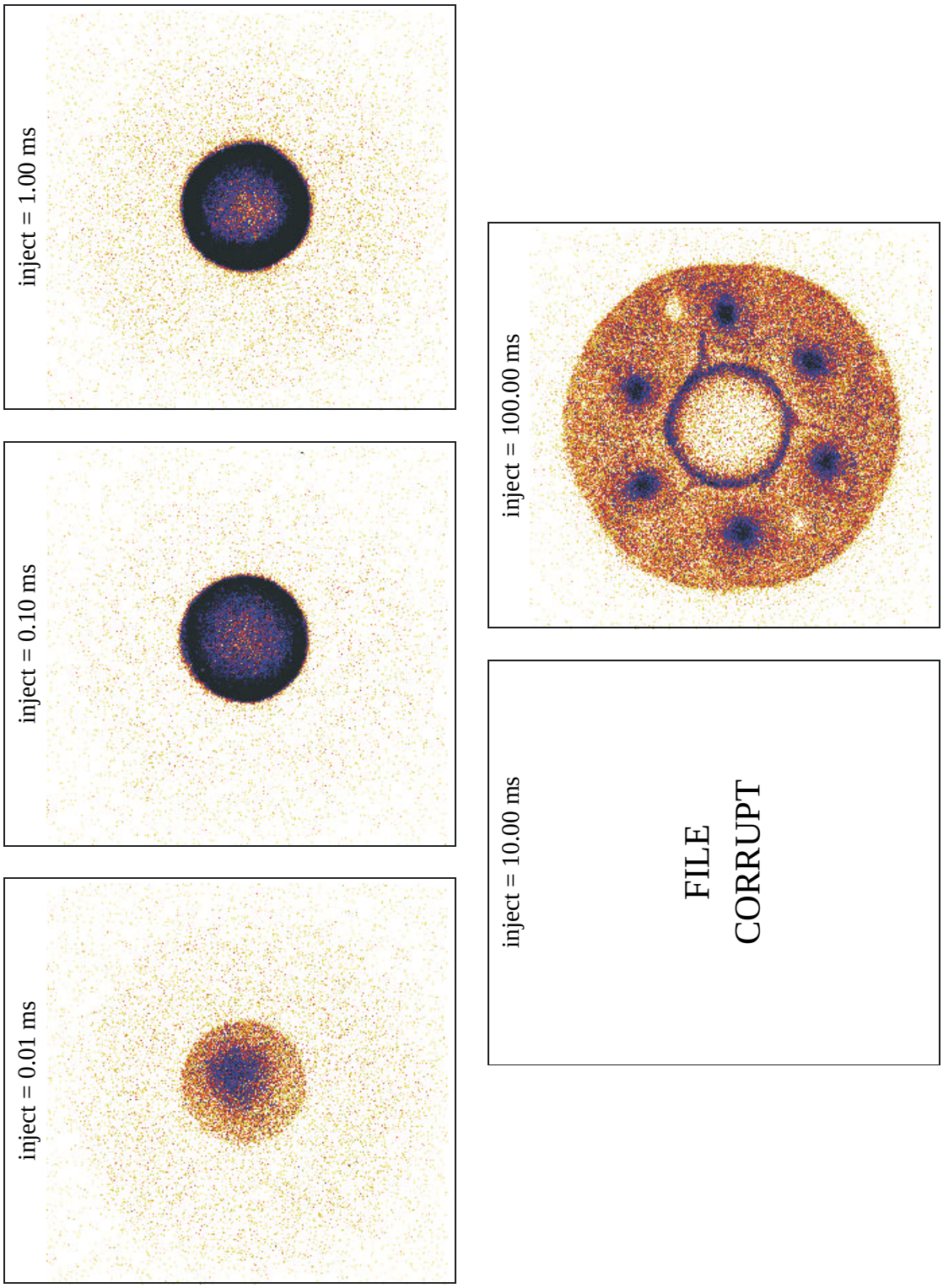

Figure 3.7: Electron Pro¯le vs Inject Time, -10 V Cathode. The pro¯le of 10.00 ms was lost due to a computer glitch. Note the extremely interesting pro¯le of 100.00 ms.

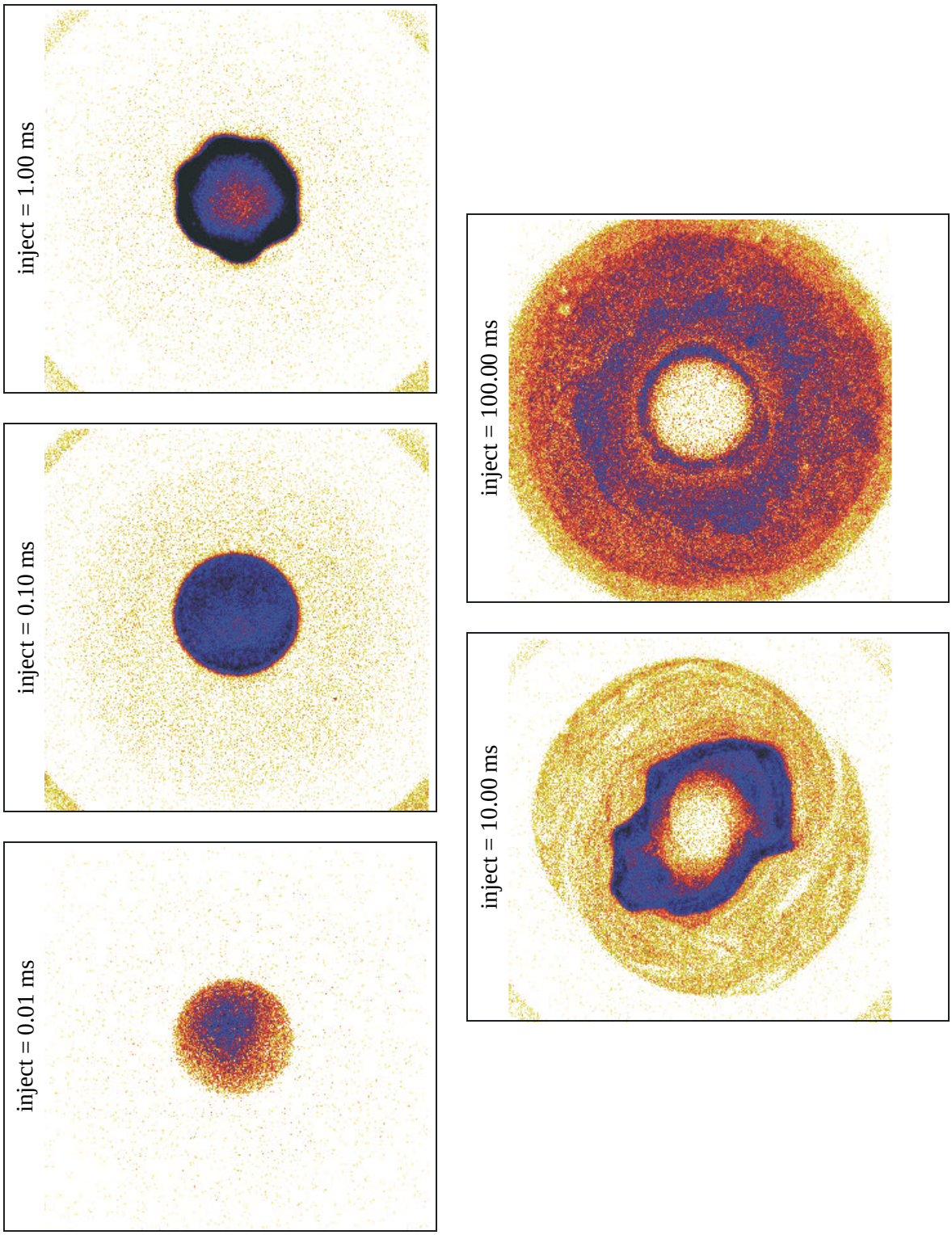

Figure 3.8: Electron Pro¯le vs Inject Time, -20 V Cathode. Note that the density has been rescaled such that these images are twice as dense compared to Figure 3.6 and Figure 3.7.

Chapter 4

Experiments on 2D Vortex Patterns

The equations governing the evolution of a strongly magnetized pure electron system are analogous to those of an ideal 2D °uid. Electron density is analogous to °uid vorticity by the Fluid Analogy (see Appendix A). Therefore, we can investigate the stability of 2D vortex patterns with magnetized electron columns. In particular, we have investigated the following cases:

- The stability of N vortices arranged in a ring.
- The stability of N vortices arranged in a ring with a central vortex.
- The stability of more complicated vortex patterns.

4.1 History

In the late 1800's, the problem of the stability of a ring of 2D vortices attracted attention because of its connection with a vortex model of atoms. Lord Kelvin [50] solved the case of three vortices, but it was not until J.J. Thomson's Adams Prize essay of 1883 [51] that the particular cases of three, four, ¯ve, six, and seven vortices were solved, with instability predicted for seven vortices. In 1931, T.H. Havelock [19] generalized the calculation to N vortices arranged in a ring (now showing that the case of seven vortices was neutrally stable with no boundary) and predicted stability criteria for the radius of an outer boundary. He

also considered the case of N vortices arranged in a ring with a ¯xed central vortex and demonstrated that a su±ciently strong central vortex could stabilize an otherwise unstable ring.

Experimentally, stable vortex patterns were ¯rst observed in super°uid ^{4}He by Yarmchuk, Gordon, and Packard in 1979 [16, 17]. In this system, quantized rectilinear vortices formed in a rotating chamber and these cooled into stable 2D vortex patterns as they interacted with the normal component of the °uid. Note that they had no control over the initial pattern and they could not test the stability of patterns directly. They got what nature gave them. This work did motivate Campbell and Zi® to computationally generate a catalog of stable 2D vortex patterns for N = 1 to 30, and for certain N up to 217 [14, 15].

We approached the problem from the nonneutral plasma point of view, where a magnetized electron column is analogous to a °uid vortex. The Photocathode Trap was designed speci¯cally to study °uid-type experiments. Because of its ability to inject controlled, complicated shapes, we were supposed to study the decay of 2D turbulence by injecting many vortices and following their subsequent mergers as the number of vortices decreased with time. Fine, Cass, Flynn, and Driscoll [18] were able to report this ¯rst by injecting the spiral of their thermionic spiral ¯lament. This spiral was unstable to the Kelvin-Helmholtz instability and therefore produced many vortices (on the order of 100). They discovered, though, that the decay of their system was sometimes arrested by the formation of stable vortex patterns. Yet they also got what nature gave them. It was about this time that the original Photocathode Trap eked into existence and we too observed the formation of stable 2D vortex patterns.

The Photocathode Trap, when working, has the advantage of being able to inject 2D vortex patterns in a controlled fashion. Besides getting what nature gives us, we can get what we want as well.

4.2 Experimental Setup

In this section, I will explain how the experimental parameters were set for these experiments:

- Magnetic Field: The dynamical time scale goes as the E £ B drift time and therefore as B. To slow this time scale as much as possible and to help suppress the smearing

that can occur during the injection of a pattern, the magnet was set to its largest possible ¯eld of 3 Tesla.

² Pattern Radius: The pattern radius for these experiments was set to be below the predicted instability radii for the di®erent patterns; therefore, all patterns have an outer radius of 0.5 cm, translating into a radius normalized to the boundary radius of 0.25. It was a goal to probe the radius stability criteria, but nonuniform photoemission in the outer regions of the photocathode made this impossible.

² Vortex Size: The vortex size was chosen to be as small as possible in order to simulate the point vortex theories under scrutiny. For the majority of experiments, the vortex radius was set at 0.05 cm, but for the pattern of 19 vortices, a radius of 0.025 cm was chosen. This essentially represents the limit of the resolution of the printer used to produce the slides and also corresponds to 4 pixels in the CCD imaging system. Note that it was not the goal here to test the stability of 2D vortex patterns composed of ¯nite sized vortices [52], though these experiments could easily be performed.

² Light Source Brightness: The brighter the light, the denser the electron columns, and therefore the brighter the phosphor image. Also, denser electron columns are less susceptible to being sheared away and are therefore easier to work with. But, the light system is immersed in the very high magnetic ¯eld and the ¯lament is subject to destructive I £ B forces. Brighter bulbs also mean hotter bulbs, which can heat the inner bore of the magnet and the vacuum chamber itself, producing a slight but noticeable pressure rise. Since I did not have an unlimited projector bulb budget, I generally ran the 82 volt bulbs at 40 volts (AC), though at times °irted with 60 volts, especially with the more complicated vortex patterns.

² Cathode Voltage: A slide would be loaded, the pattern centered in the trap, and then the cathode voltage was tuned to produce a vortex pattern as nearly uniform as possible. The cathode voltages were on the order of -5 volts.

² Inject Time: The inject time was chosen to be as fast as possible (5 ¹s) in order to suppress the phenomena of pattern smearing (see Chapter 3).

² Trapping Gates Voltage: The gate voltages were set as close to the cathode voltage as possible to allow for the longest possible electron columns and to suppress ¯nite

length blurring e®ects (typically -20 volts).

The above parameters typically injected electron columns with a density of 1 £ 10^7 cm^{-3} and a temperature of 1 eV, corresponding to a Debye length of 0.20 cm.

4.3 Experimental Procedure

1. Slides of the desired vortex patterns are printed out on transparency ¯lm with an ink jet printer and attached to aluminum holders.
2. A given slide is loaded into the light source and the pattern is centered to the known trap center using the CCD camera.
3. The cathode voltage is adjusted to produce a pattern of uniform brightness. Uniformity is on the 10 % level.
4. The hold time is varied and the time for one bulk rotation (T_B) is measured.
5. The hold time is varied and the lifetime for the pattern (T_L) is determined and the mode of death is noted. In general, there are two distinct modes of pattern death:
   (a) Point Vortex: Essentially the repositioning of the vortices into a new and distinct pattern. This mode is symptomatic of patterns that are truly unstable initially.
   (b) Finite Size: The merging, shearing, or fading of vortices, all outside the realm of point vortex dynamics. This is often the mode of death for initially stable vortex patterns and dominates only after hundreds of bulk rotations, when collisions become signi¯cant.
6. New formed stable vortex patterns are noted.

4.4 N Vortices Arranged in a Single Ring

The problem of N vortices arranged in a ring was solved by Havelock. He predicted the following:

- N < 7: The ring is stable.
- N = 7: The ring is neutrally stable with no boundary, but unstable with a boundary.

- N > 7: The ring is unstable.

Here I present experimental data for N = 2 to 10 vortices and demonstrate agreement with the theory (see Figure 4.1):

- N < 7: (see Figure 4.2) These patterns live for over 1000 bulk rotations, a time that is of the order of over a second. The mode of death is \Finite Size", as the vortices fade away. These long times correspond to many collisional times (on the order of 10 ms) and are considered outside the realm of The Fluid Analogy. An example of such an evolution is presented for 5 vortices (see Figure 4.5), where at 1000 bulk rotations the vortices are noticeably weaker, and at 4000 bulk rotations one vortex has faded away altogether, leaving 4 weaker vortices. Eventually, these 4 fade away leaving 1 at 10000 bulk rotations (10 s), and even that will eventually dissipate.

- N = 7: (see Figure 4.3) This pattern lives for several hundred bulk rotations, a lifetime that can be considered metastable. The normalized ring radius is 0.25 and so the e®ects of the boundary are small (remember, N = 7 is neutrally stable with no boundary). The mode of death here, though, is \Point Vortex", unlike for N < 7. Often, one vortex will move into the center, forming a new pattern of 6 vortices in a ring with 1 central vortex. This is actually the only pattern predicted stable for 7 vortices by Campbell and Zi®, and here is observed to live for 1000 bulk rotations.

- N > 7: (see Figure 4.4) These patterns live on the order of 1 bulk rotation. The mode of death is \Point Vortex". These patterns are clearly unstable and example evolutions are given for N = 8, N = 9, and N = 10. For N = 8 (see Figure 4.6), the pattern quickly rearranges into 7 vortices in a ring with 1 central vortex. This is the only pattern predicted stable for 8 vortices by Campbell and Zi®, and here is observed to live for 1000 bulk rotations. For N = 9 (see Figure 4.7), the pattern quickly rearranges into 8 vortices in a ring with 1 central vortex. This is the most stable pattern predicted for 9 vortices by Campbell and Zi®. For N = 10 (see Figure 4.8), the pattern again rearranges, but the motion brings 2 vortices too close together and a merger is observed at 1.00 ms. This merger event can only happen with ¯nite sized vortices, as I have in my experiment (it is impossible to conserve energy and momentum in the merger of two point vortices).

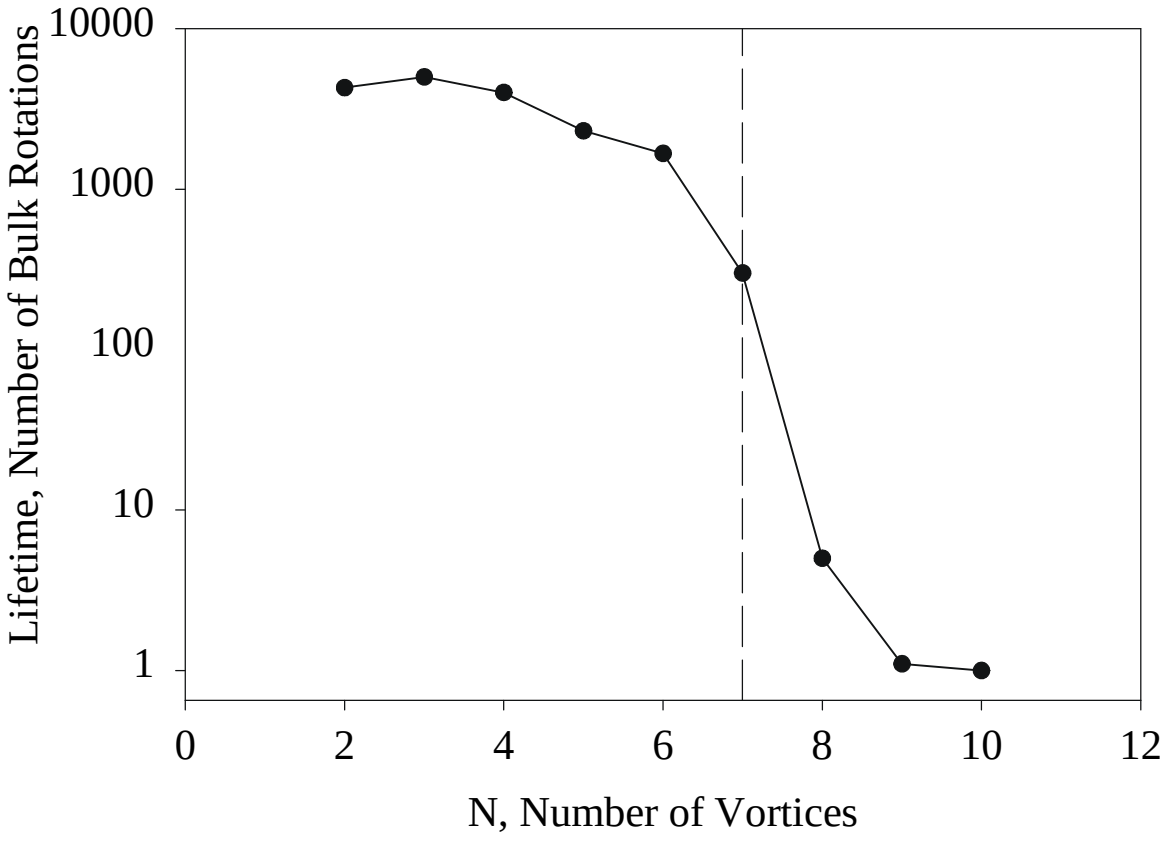

Figure 4.1: Lifetime versus N, for N vortices arranged in a ring.

A note should be made about the evolution of one pattern into another stable pattern. This evolution involves the exchange of energy. In the super°uid helium experiments, the interaction between the super°uid and normal components of the °uid provides the mechanism by which vortices can \cool" into new stable patterns. Here, in these electron systems, the mechanism is not obvious, but could be do to e®ects outside The Fluid Analogy, such as collisions with the background gas or ¯nite length e®ects.

4.5 N Vortices Arranged in a Single Ring with a Central Vortex

The problem of N vortices arranged in a ring with a ¯xed central vortex was solved by Havelock. The case of a free central vortex, as I have experimentally, has been considered by a number of authors, including Morikawa and Swenson [53] and Campbell [54]. Freeing

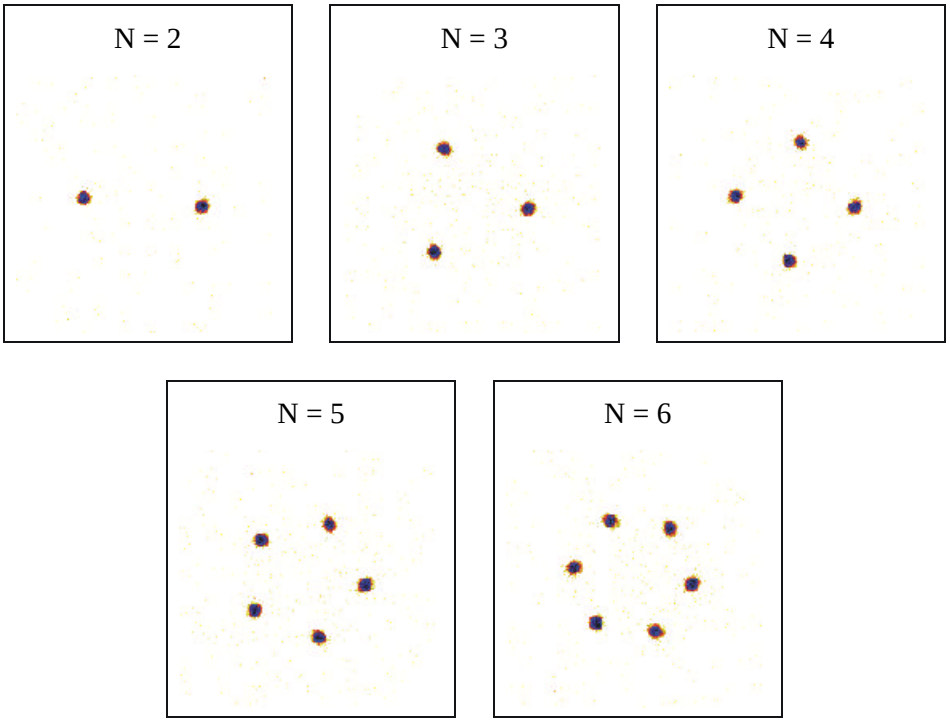

Figure 4.2: N < 7 initial states, stable for over 1000 bulk rotations.

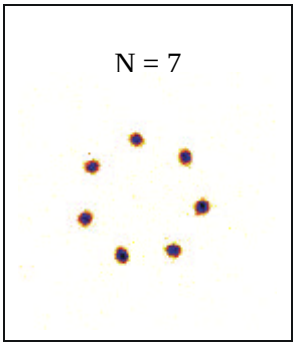

Figure 4.3: N = 7 initial state, stable for on the order of 100 bulk rotations.

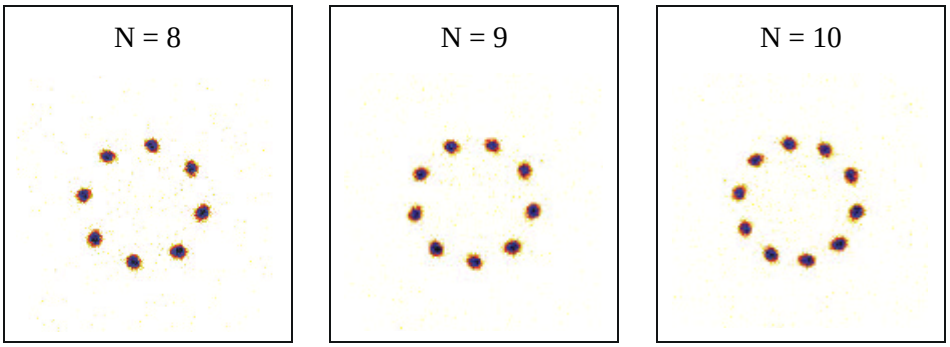

Figure 4.4: N > 7 initial states, stable for on the order of 1 bulk rotation.

the central vortex allows it to move o® center and thereby introduces an upper stability limit on the central vortex's total circulation. The lower limit corresponds to the ring itself going unstable.

Recently, Lansky and O'Neil [55] have analyzed the e®ect of a boundary on the central vortex's stability limits. Note that in these experiments, the vortex ring's small normalized radius a®ects the stability limits by less than 1 %, well below experimental control.

Experimentally, it is di±cult to control the density of the electron columns. It is easy, though, to manipulate the size of the central vortex simply by manipulating the size of the slide image. In this manner, central vortices of various circulations were injected along with rings of vortices. This method of course introduces the possibility of ¯nite vortex size problems. Experimentally, I observed that the method worked well for central vortices under a certain limit.

For these experiments, ° is the central vortex's strength normalized by a ring vortex's strength.

Here I present experimental data for N = 3 + 1 through 10 + 1 vortices and demonstrate general agreement with the theory:

- N = 3 + 1: (see Figure 4.9 and Figure 4.10) The initial vortex patterns are presented, as well as the stable patterns that the initially unstable patterns evolve into. The patterns go unstable for ° > 1 and they go unstable by the central vortex, both as predicted. Note the new formed stable patterns with the ring vortices grouping together to compensate the displaced stronger central vortex.

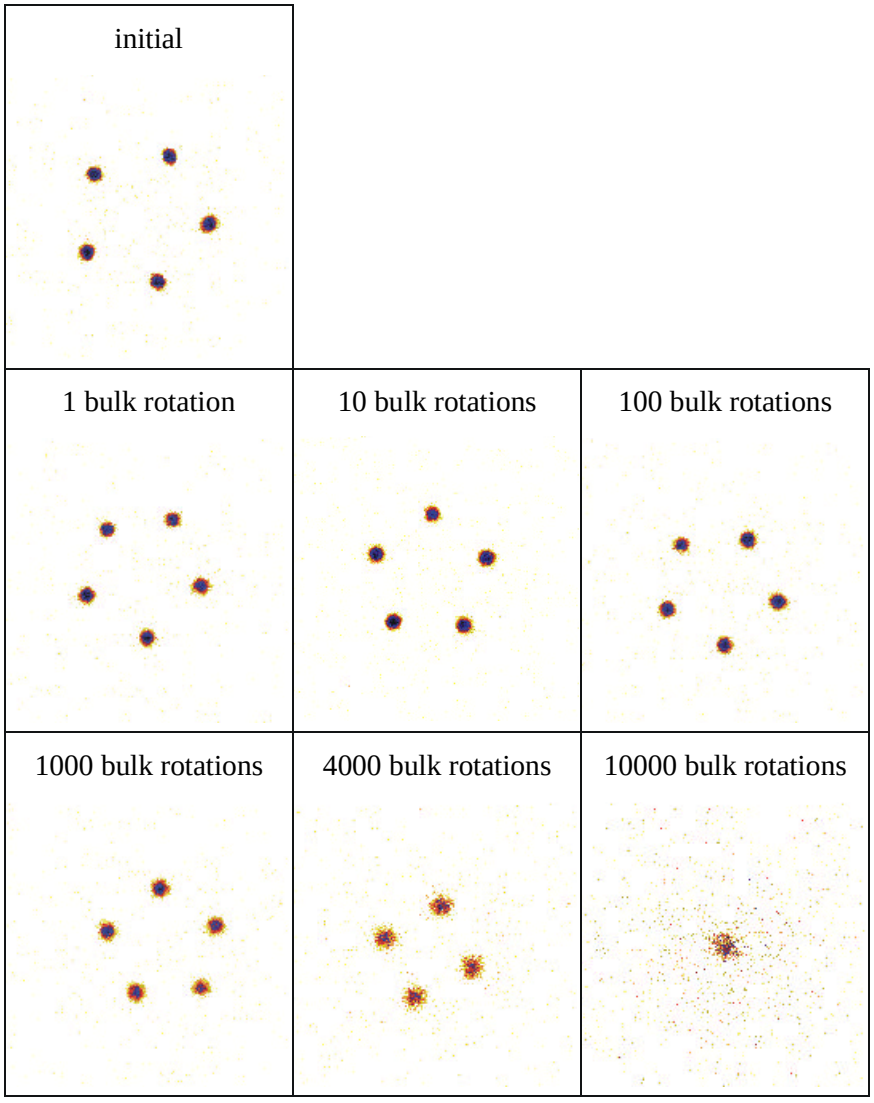

Figure 4.5: N = 5 evolution.

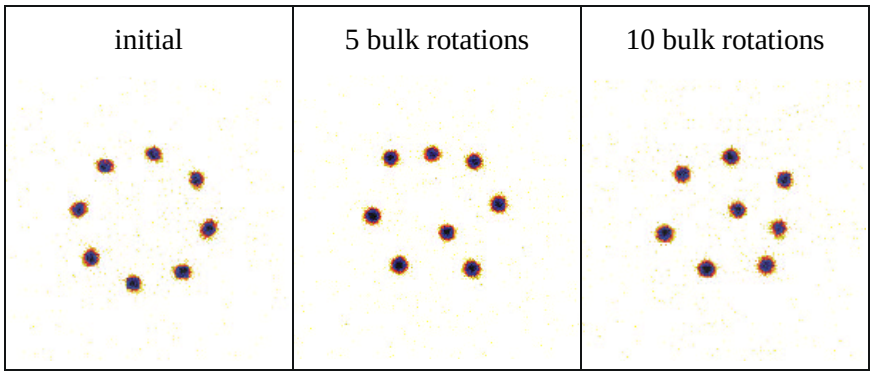

Figure 4.6: N = 8 evolution.

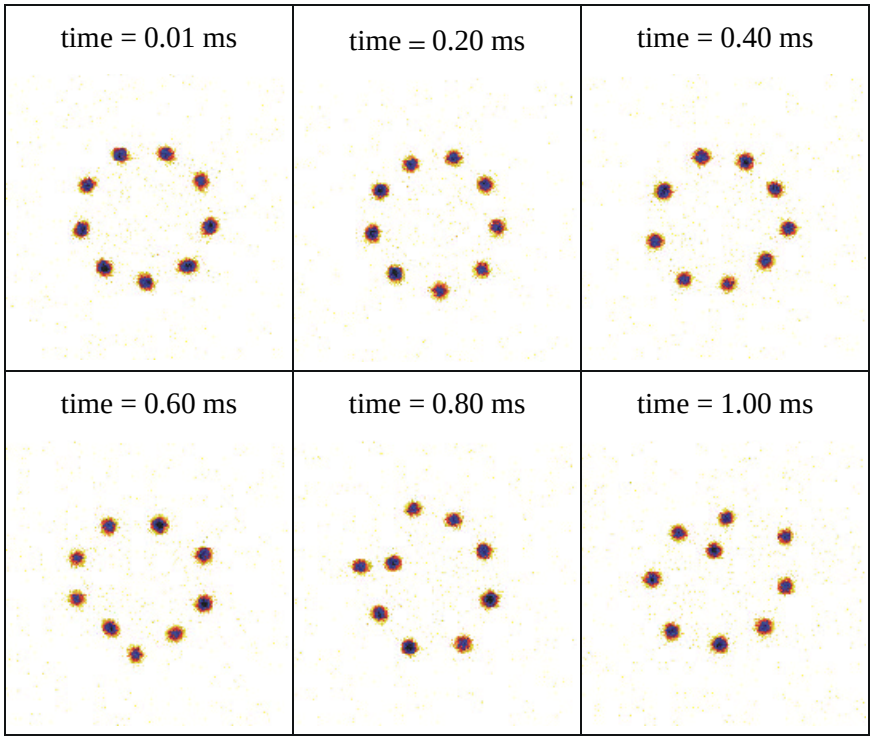

Figure 4.7: N = 9 evolution.

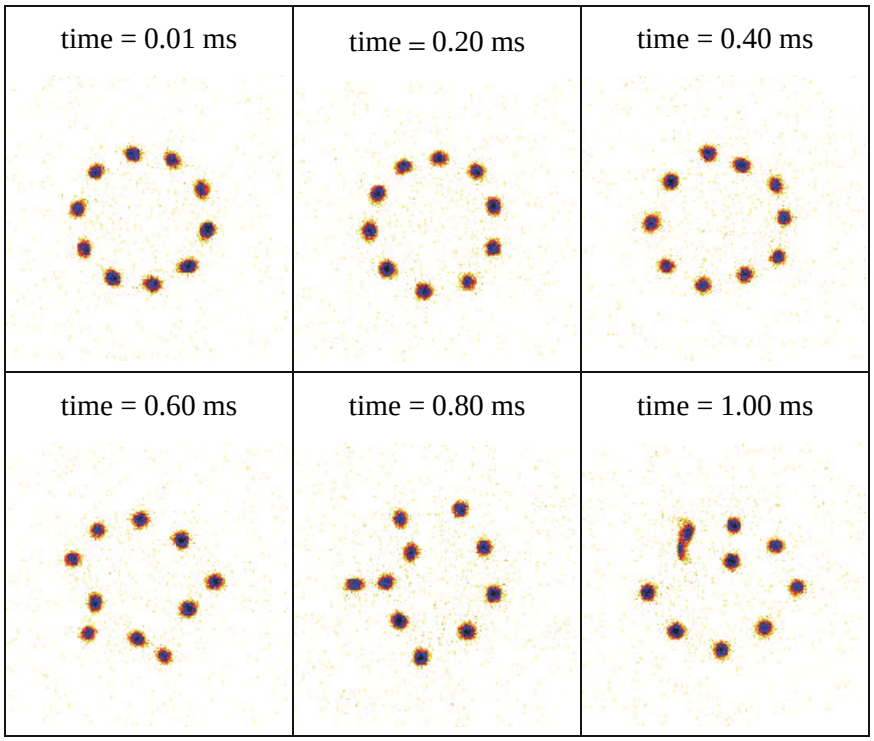

Figure 4.8: N = 10 evolution.

- N = 4 + 1: (see Figure 4.11 and Figure 4.12) Again, the initial vortex patterns are presented, as well as the stable patterns that the initially unstable patterns evolve into. And again, there is fairly close agreement with the theory and agreement that they go unstable by the central vortex. Note the for ° = 1, the initial pattern lives for 50 bulk rotations, but evolves into 5 vortices in a ring that lives for 500 bulk rotations. Both patterns for 5 vortices are predicted to be stable.

- N = 5 + 1: (see Figure 4.13 and Figure 4.14) Here, the agreement with theory is not as good and could represent a limitation of varying the strength of a theoretically point vortex by varying the size of a uniform vortex. Also, it is always easy to make a pattern unstable, but much harder to determine if it is truly stable (by tweaking voltages, balancing photoemission, centering the pattern).

- N = 6 + 1: (see Figure 4.15 and Figure 4.16) Again, the agreement is not as good. The upper stability limit is no longer accessible with the current setup.

- N = 7 + 1: (see Figure 4.17 and Figure 4.18) Excellent agreement with theory returns, as the lower stability limit is now being probed.

- N = 8 + 1: (see Figure 4.19 and Figure 4.20) Again, excellent agreement with theory. For ° = 0, less than the lower stability limit, the ring vortices go unstable as predicted. Here they rearrange into 7 vortices in a ring plus 1 central vortex, the predicted stable pattern for 8 vortices.

- N = 9 + 1: (see Figure 4.21 and Figure 4.22) Again, excellent agreement with the theory. For ° = 0, this time, no stable pattern emerges.

- N = 10 + 1: (see Figure 4.23 and Figure 4.24) More excellent agreement with theory. For ° = 0, no stable pattern emerges. But, for ° = 1 a stable pattern does emerge that is predicted by Campbell and Zi®, and corresponds to 11_2 in their catalog.

In summary, the technique produced good agreement with the theory. The agreement was better when probing the lower stability limits than when probing the upper stability limits, and this is probably due to experimental limitations.

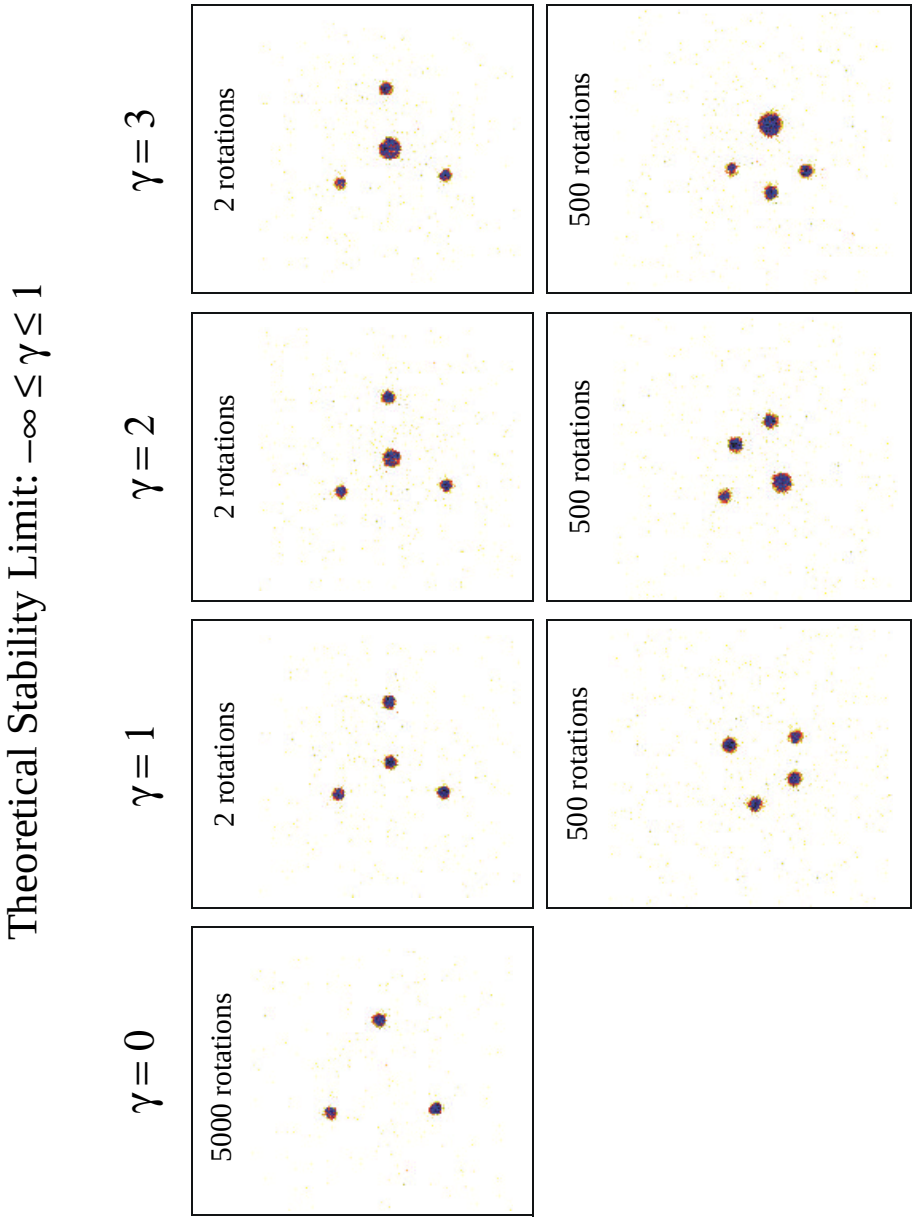

Figure 4.9: N = 3 + 1 vortex patterns.

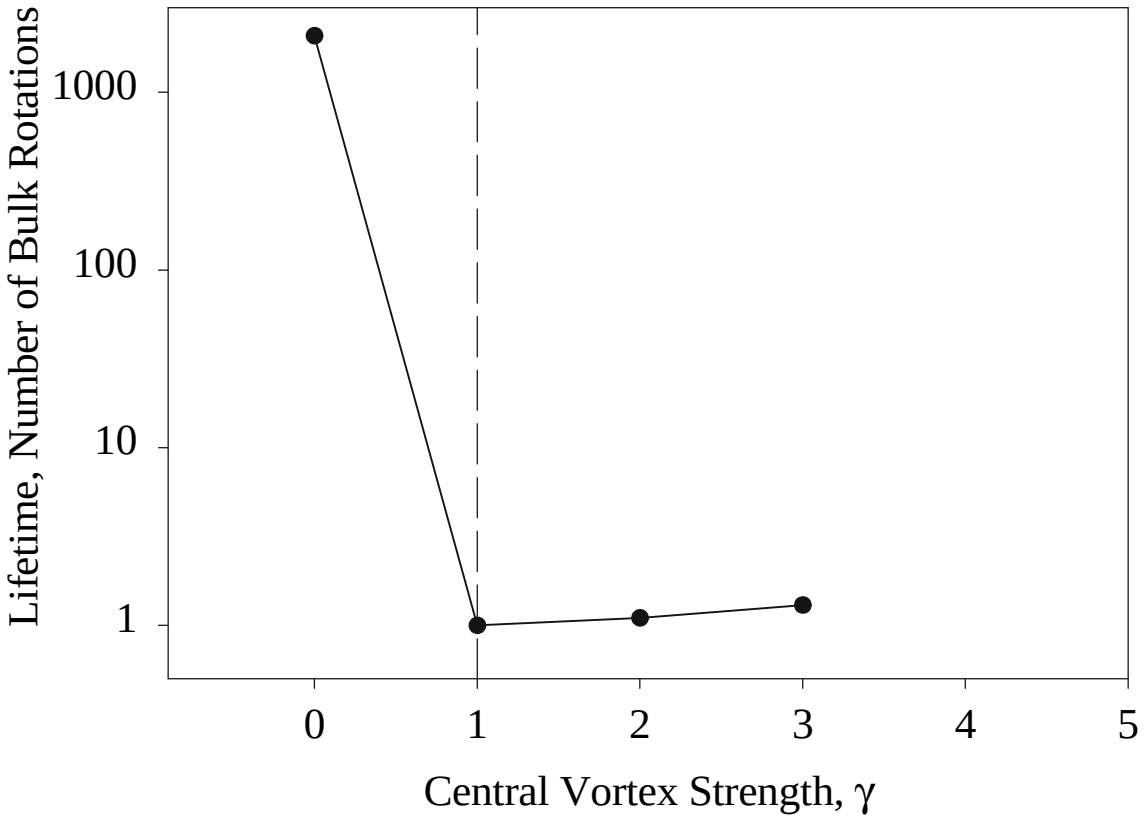

Figure 4.10: Lifetime versus ° for N = 3 + 1. The theoretical upper stability limit for ° is shown as the dashed line.

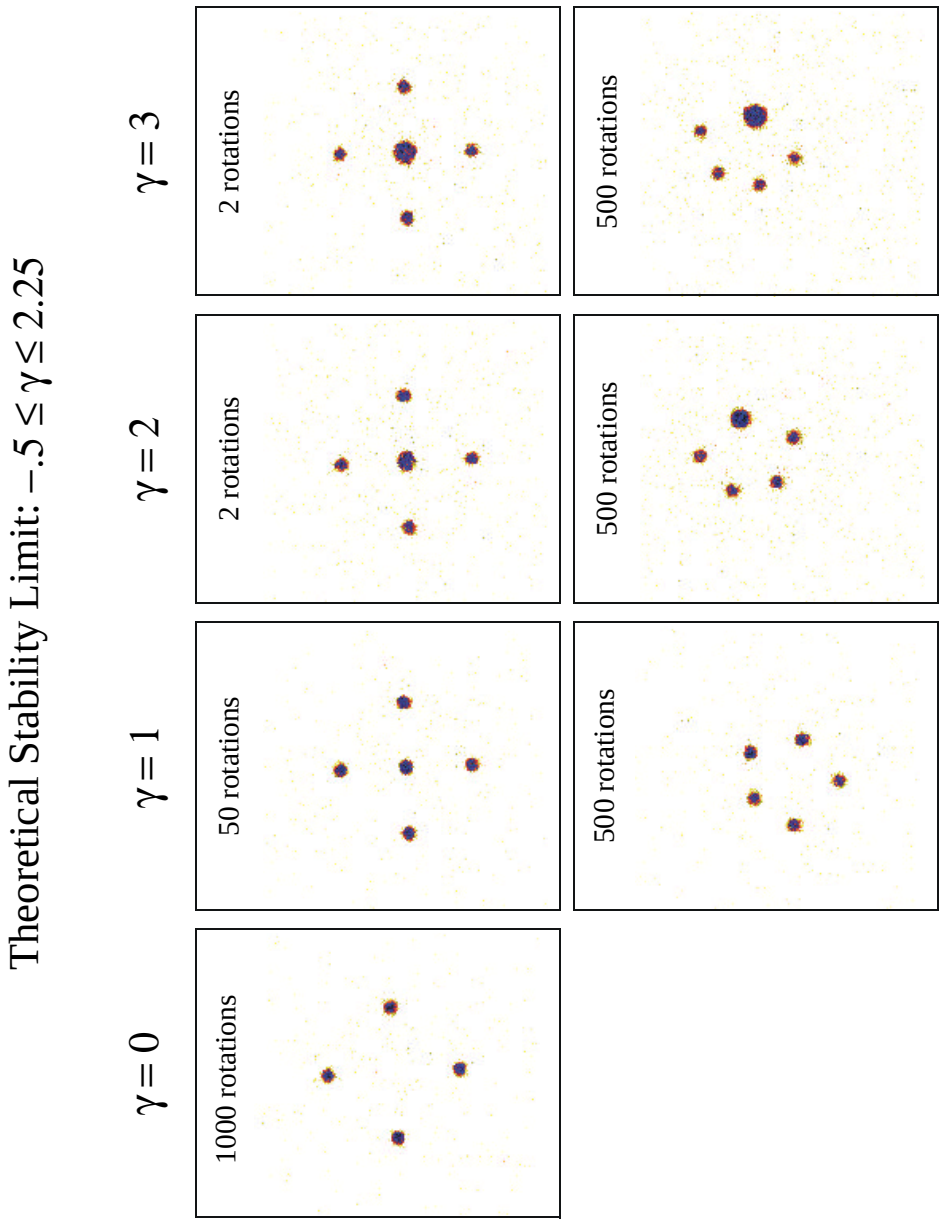

Figure 4.11: N = 4 + 1 vortex patterns.

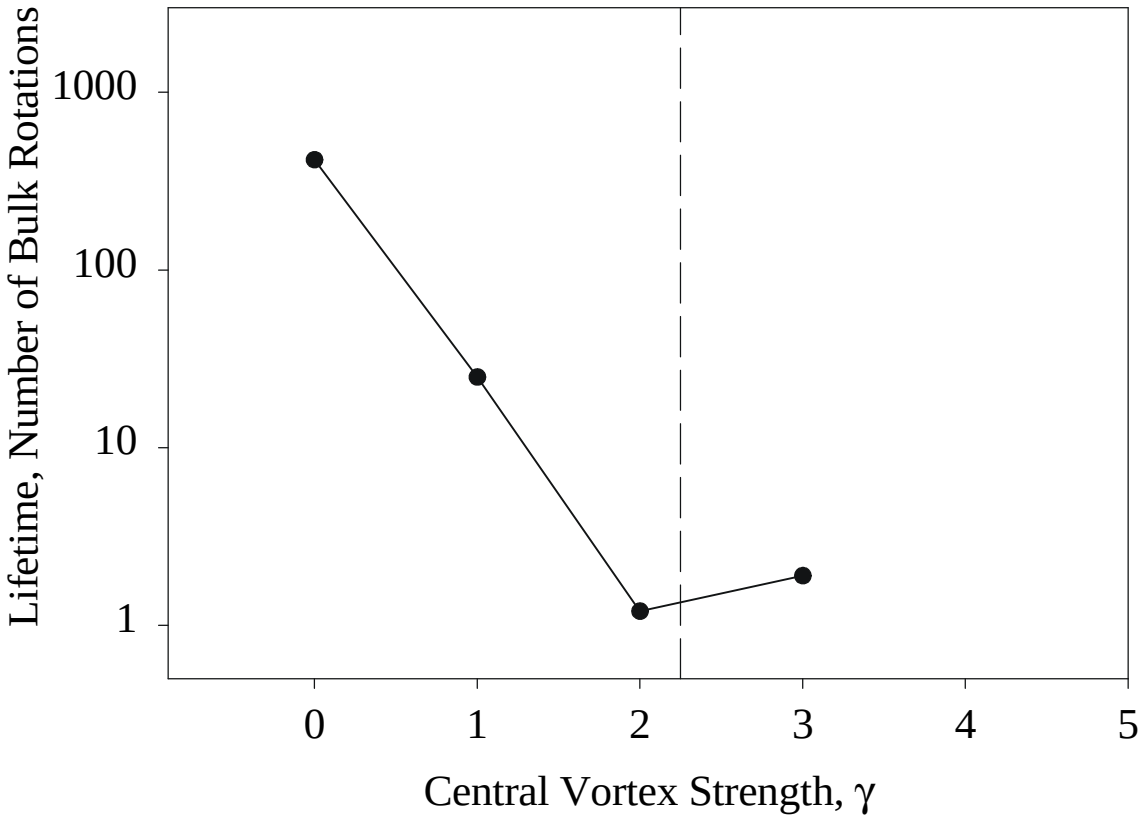

Figure 4.12: Lifetime versus ° for N = 4 + 1. The theoretical upper stability limit for ° is shown as the dashed line.

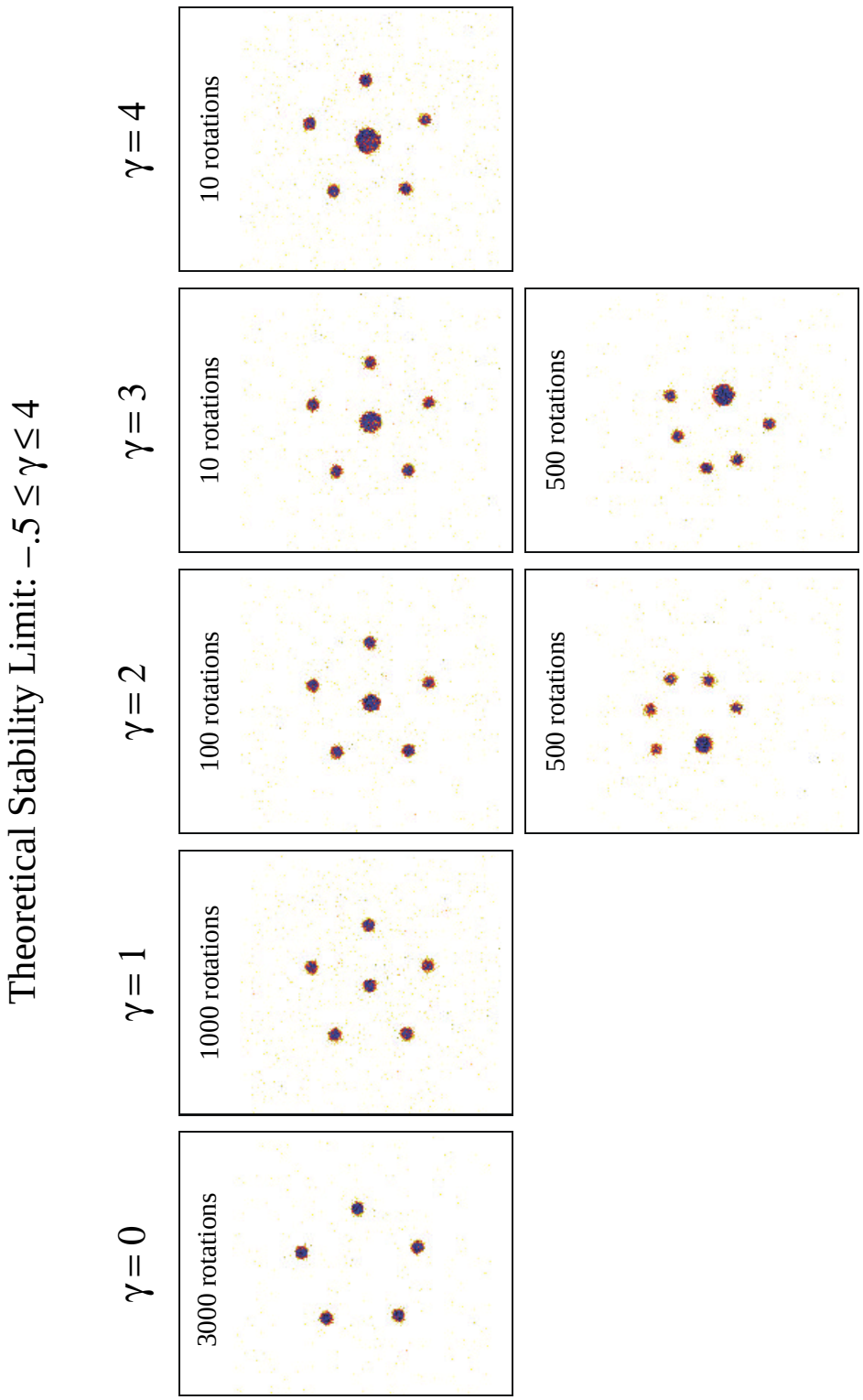

Figure 4.13: N = 5 + 1 vortex patterns.

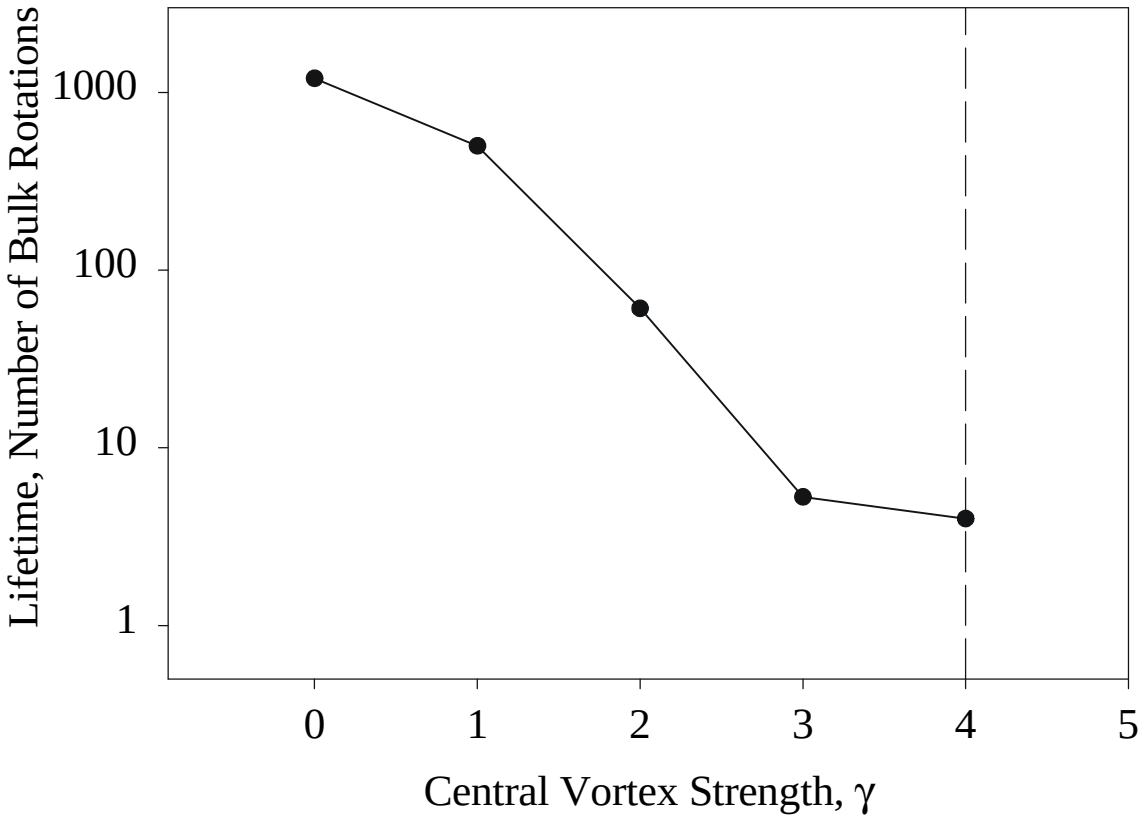

Figure 4.14: Lifetime versus ° for N = 5 + 1. The theoretical upper stability limit for ° is shown as the dashed line.

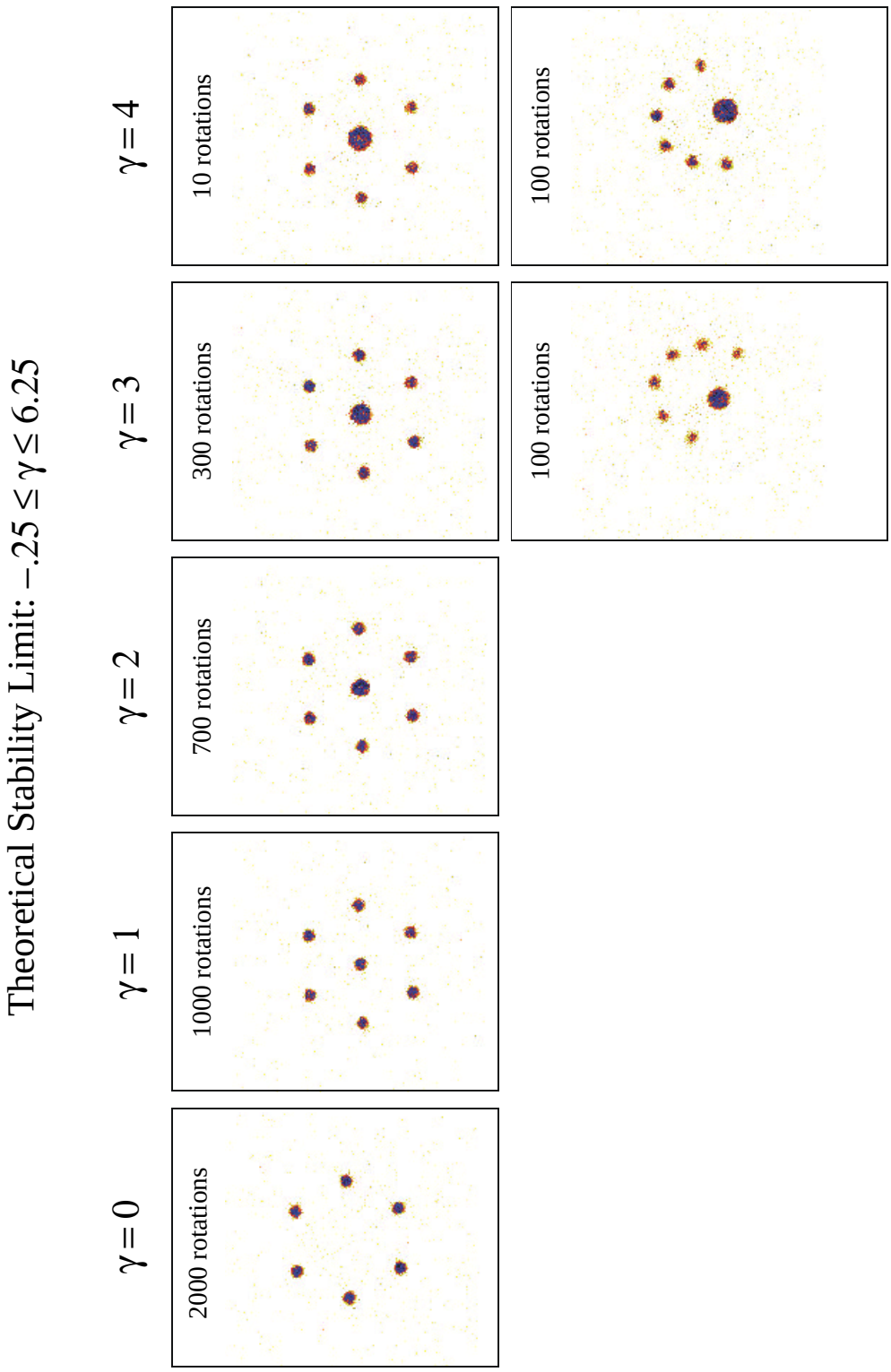

Figure 4.15: N = 6 + 1 vortex patterns.

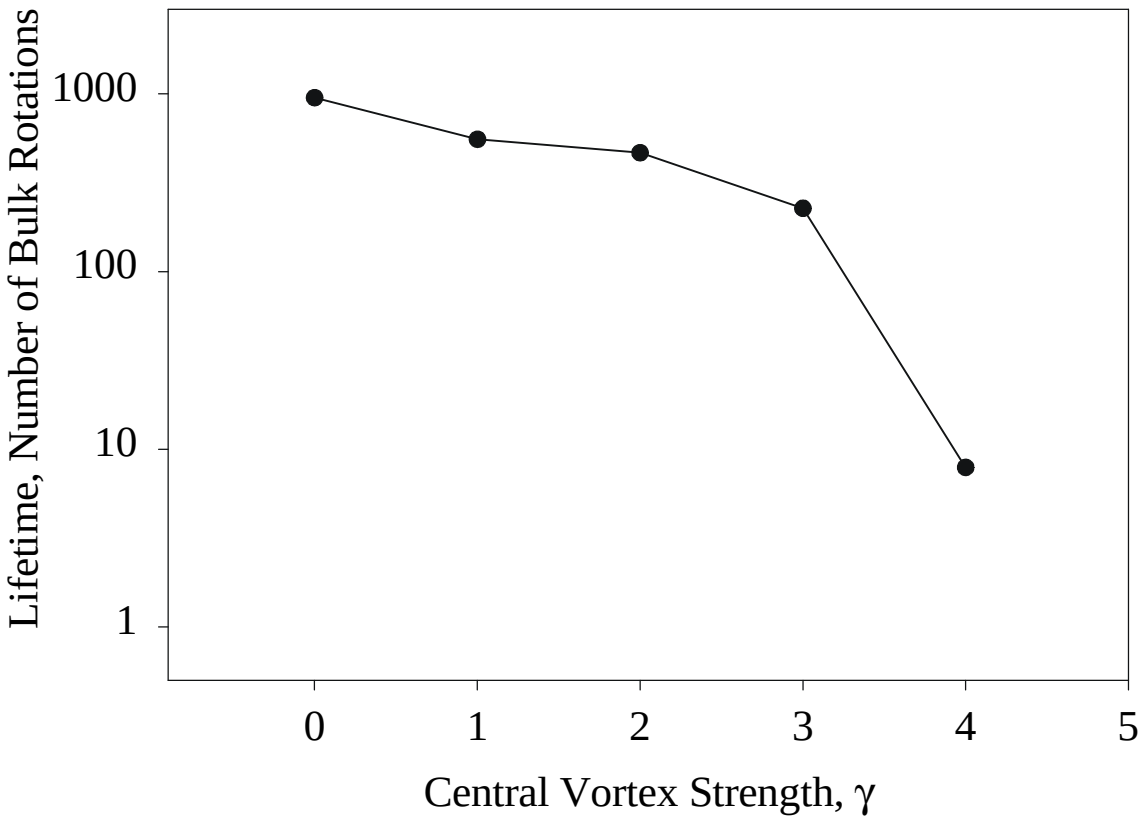

Figure 4.16: Lifetime versus ° for N = 6 + 1.

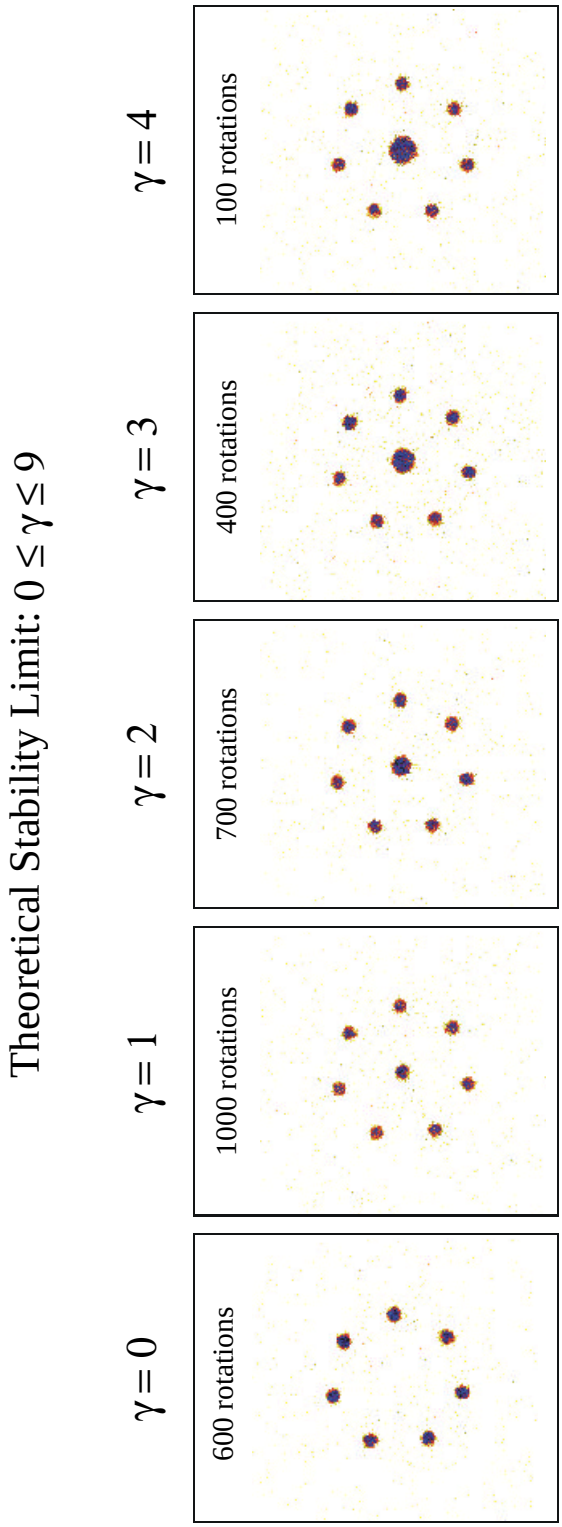

Figure 4.17: N = 7 + 1 vortex patterns.

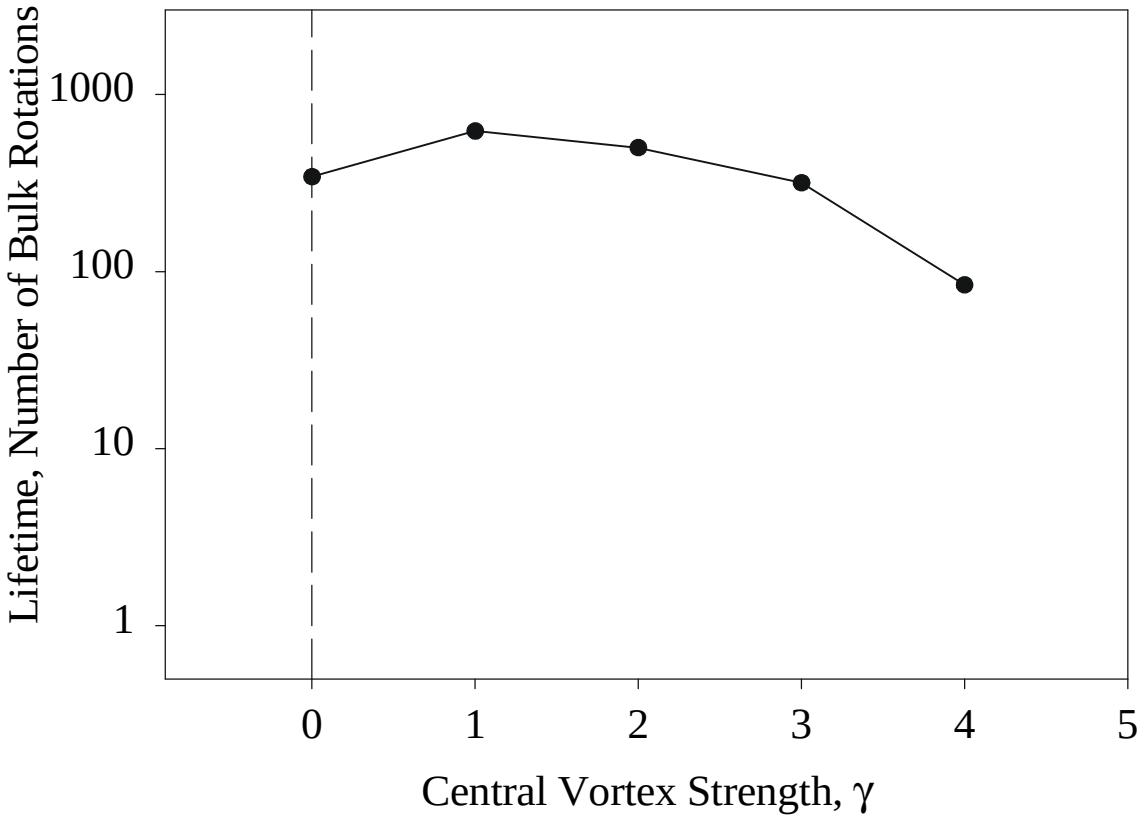

Figure 4.18: Lifetime versus ° for N = 7 + 1. The theoretical lower stability limit for ° is shown as the dashed line.

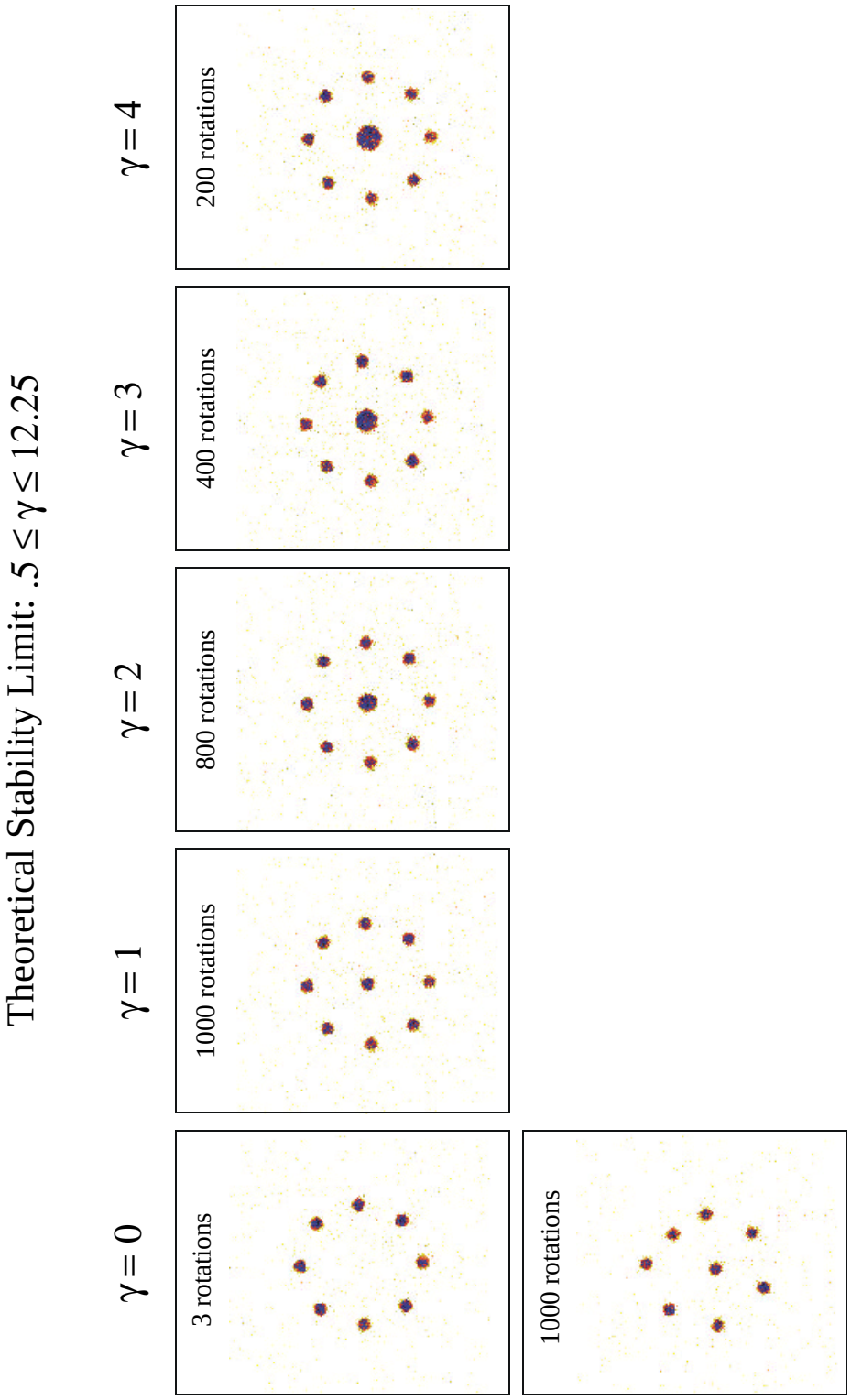

Figure 4.19: N = 8 + 1 vortex patterns.

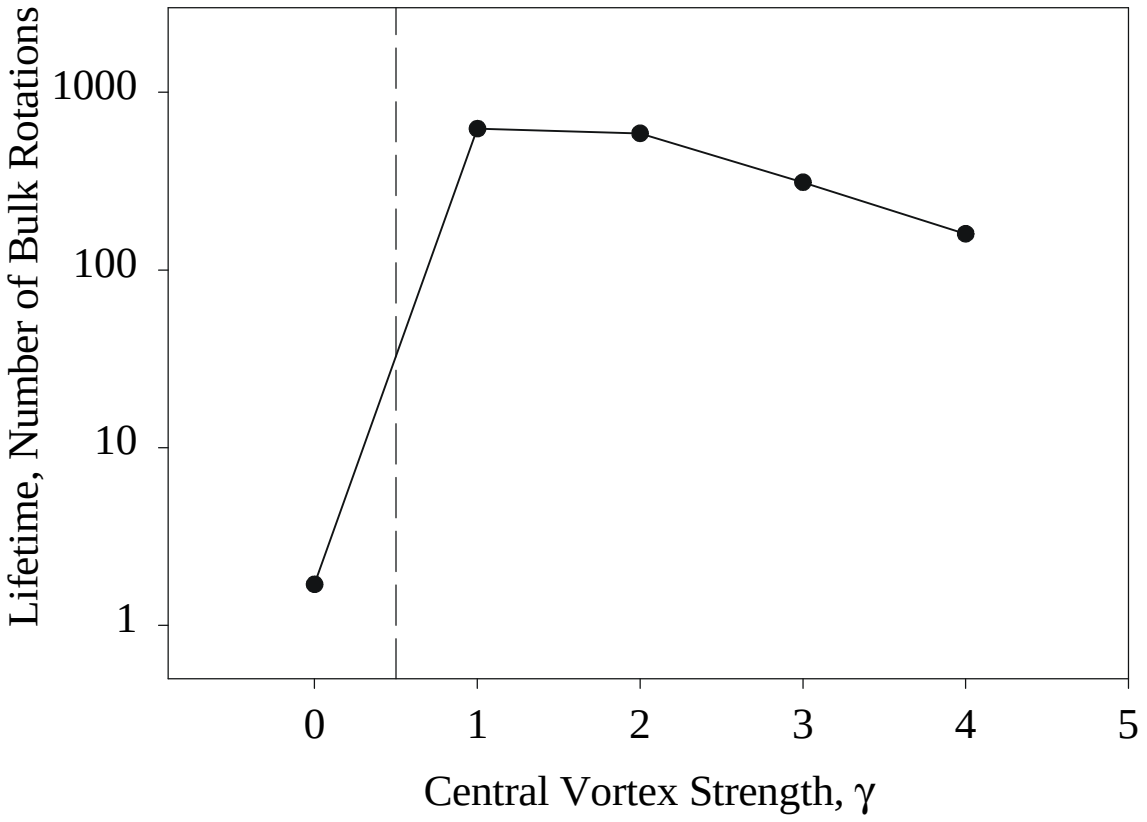

Figure 4.20: Lifetime versus ° for N = 8 + 1. The theoretical lower stability limit for ° is shown as the dashed line.

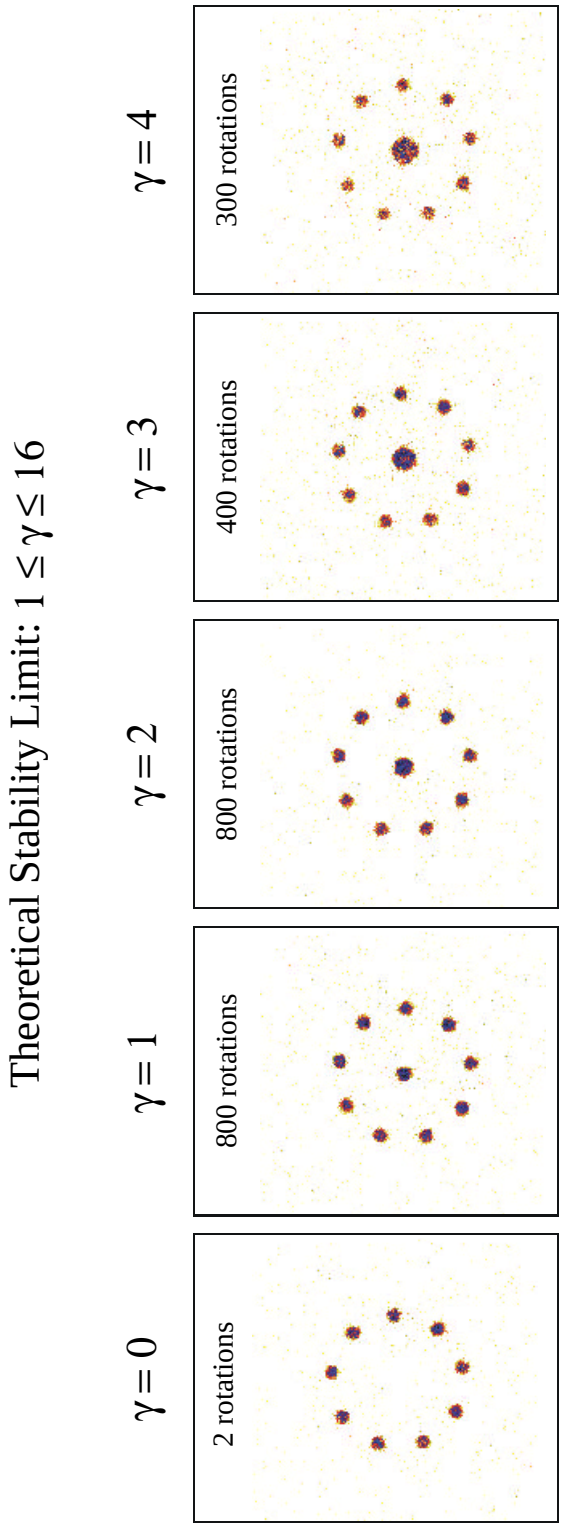

Figure 4.21: N = 9 + 1 vortex patterns.

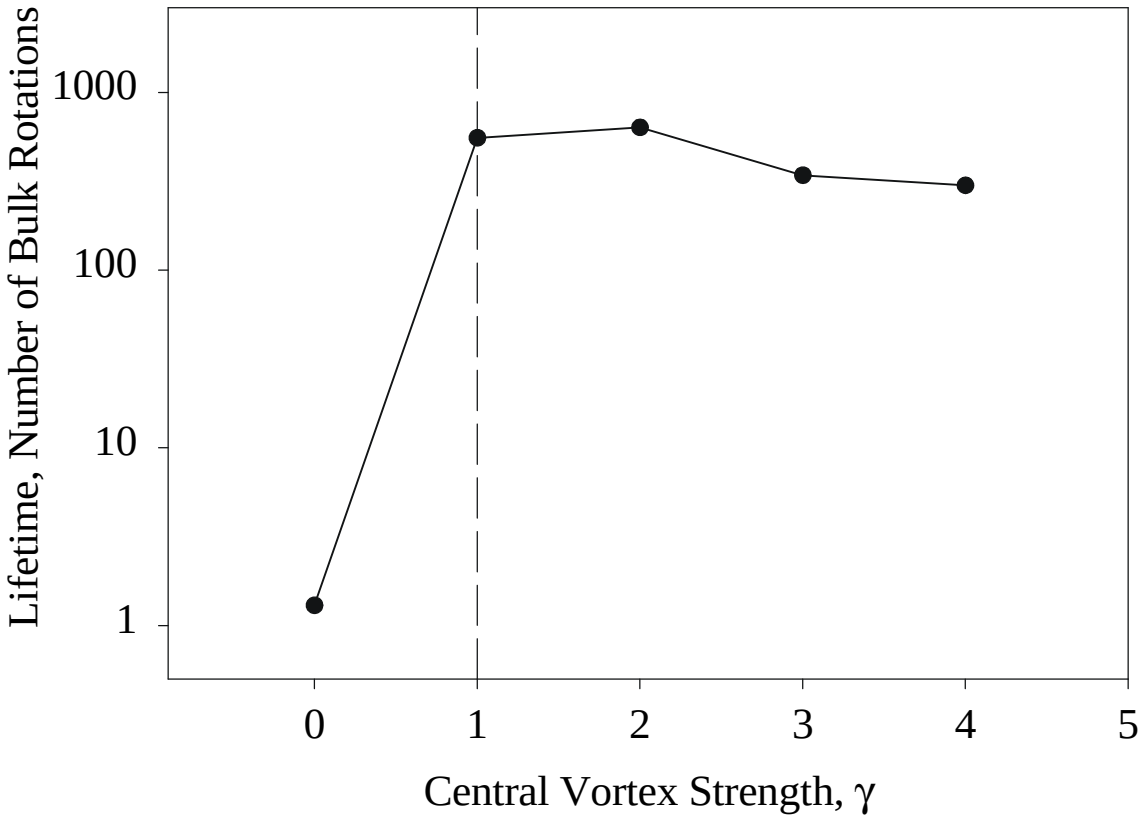

Figure 4.22: Lifetime versus ° for N = 9 + 1. The theoretical lower stability limit for ° is shown as the dashed line.

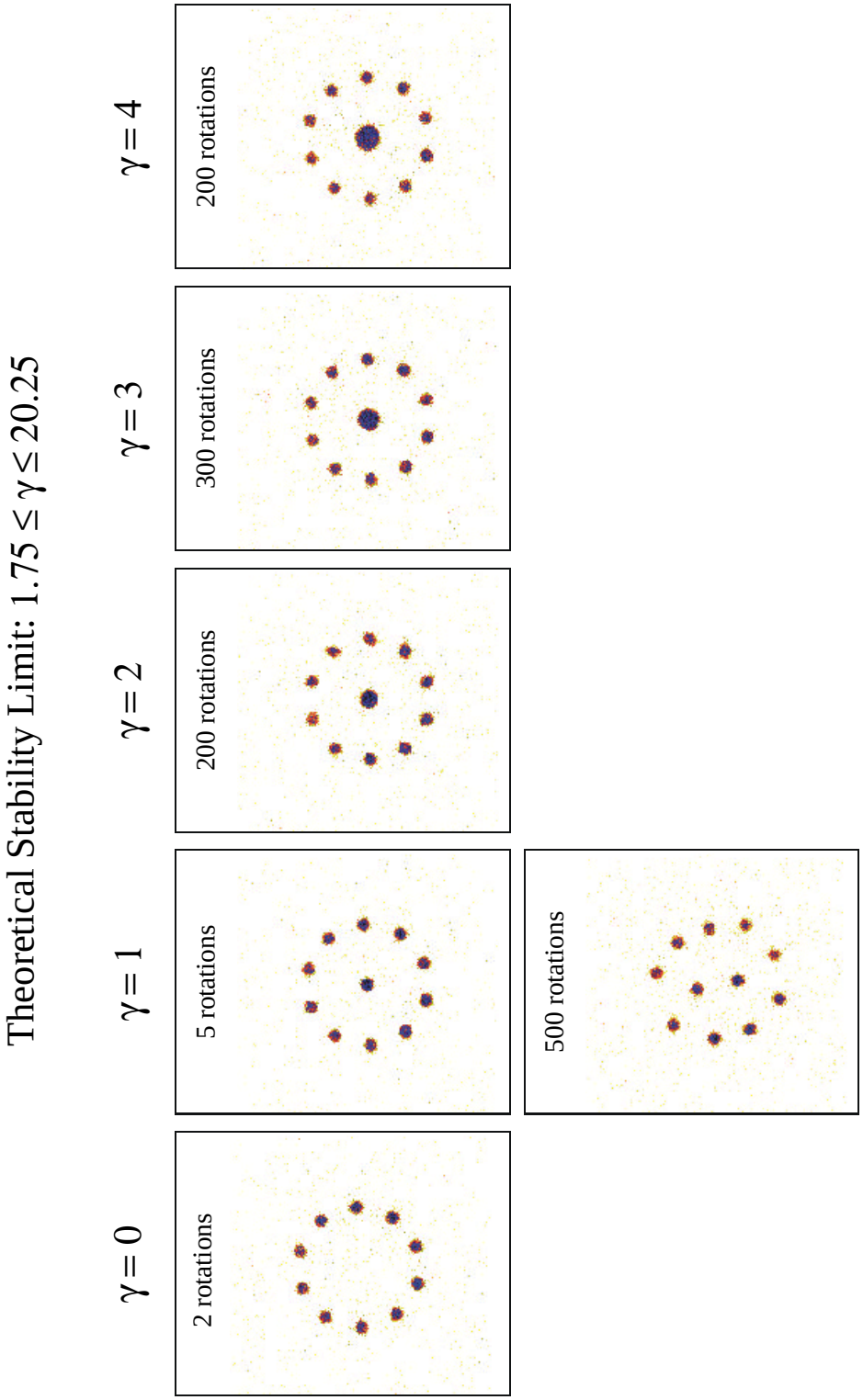

Figure 4.23: N = 10 + 1 vortex patterns.

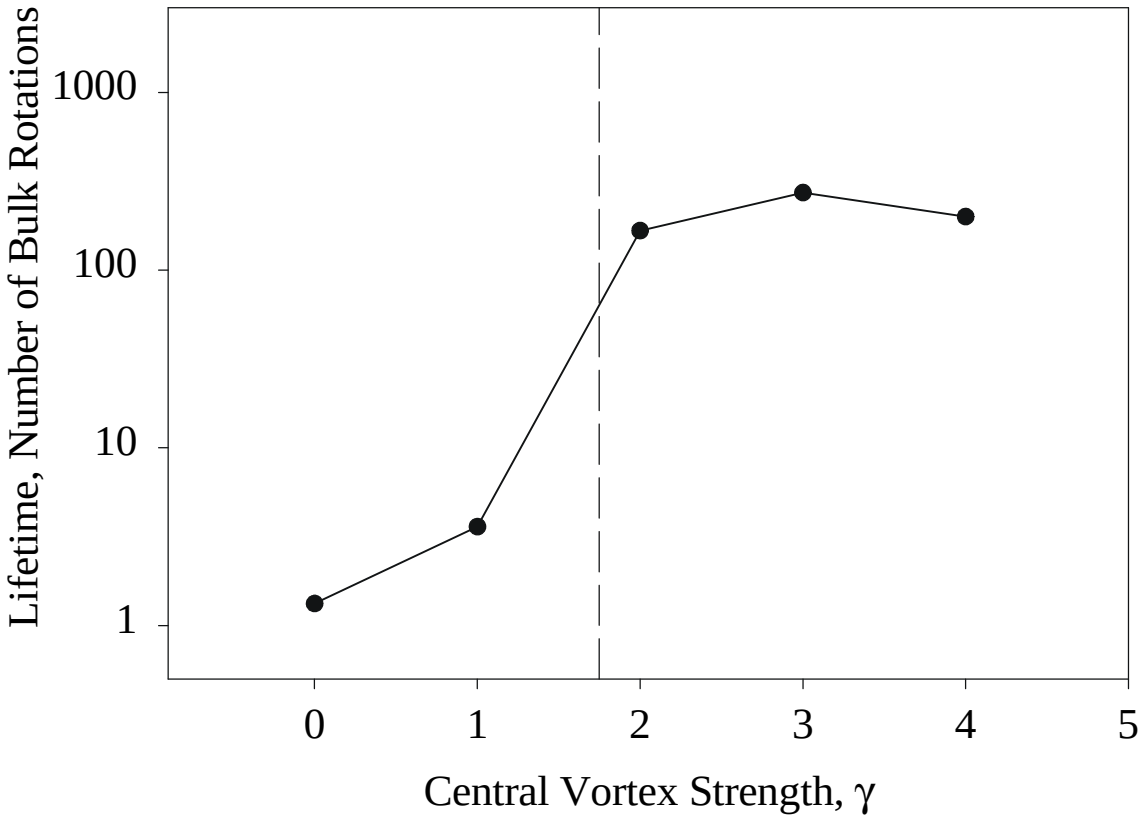

Figure 4.24: Lifetime versus ° for N = 10 + 1. The theoretical lower stability limit for ° is shown as the dashed line.

4.6 Campbell and Zi® Patterns

2D vortex patterns are of course not constrained to a ring. Campbell and Zi® have computationally generated a catalog of stable 2D vortex patterns where all the vortices have the same strength. Here I tested the stability of several of these patterns (the pattern designation is from Campbell and Zi®'s catalog):

- 10_1: (see Figure 4.25) This pattern lived for 700 bulk rotations, but was sometimes found in a 10_1 ¡ 10_2 hybrid pattern. The 10_2 pattern corresponds to having the central 2 vortices being collinear with 2 opposing ring vortices. Experimentally, it is di±cult to distinguish these patterns.

- 11_1: (see Figure 4.26) This pattern lasted for 400 bulk rotations. Remember that the 11_2 pattern was observed in the evolution of N = 10 + 1 for ° = 1 (see Figure 4.23).

- 12_1: (see Figure 4.27) This pattern lasted for 1000 rotations and was di±cult to distinguish from 12_2, which corresponds to the central 3 vortices being rotated slightly with respect to the outer vortices.

- 19_1: (see Figure 4.28) This fairly complicated pattern lasted for 100 bulk rotations and represents the ¯rst pattern controllably created outside a computer with vortices at three radii. To inject a stable version of 19_1, I needed to create smaller, denser electron columns. So, the vortex radius was reduced to 0.025 cm and the light bulb was run at 60 volts.

Another pattern that I tested was for 6 vortices (see Figure 4.29). This pattern is not found in Campbell and Zi®'s catalog, but emerged from a maximum entropy theory developed by Jin and Dubin [56] to predict stable vortex patterns in a pure electron system. Jin reports that this pattern is not very stable and here I could only get it to survive for 20 bulk rotations. Typically, I found that unstable patterns last on the order of 1 bulk rotation, whereas stable patterns lasted for over 100 bulk rotations; therefore, 20 bulk rotations is metastable.

4.7 Summary

I have demonstrated the advantage of using a Malmberg-Penning Trap with a photocathode to study the stability of 2D vortex patterns:

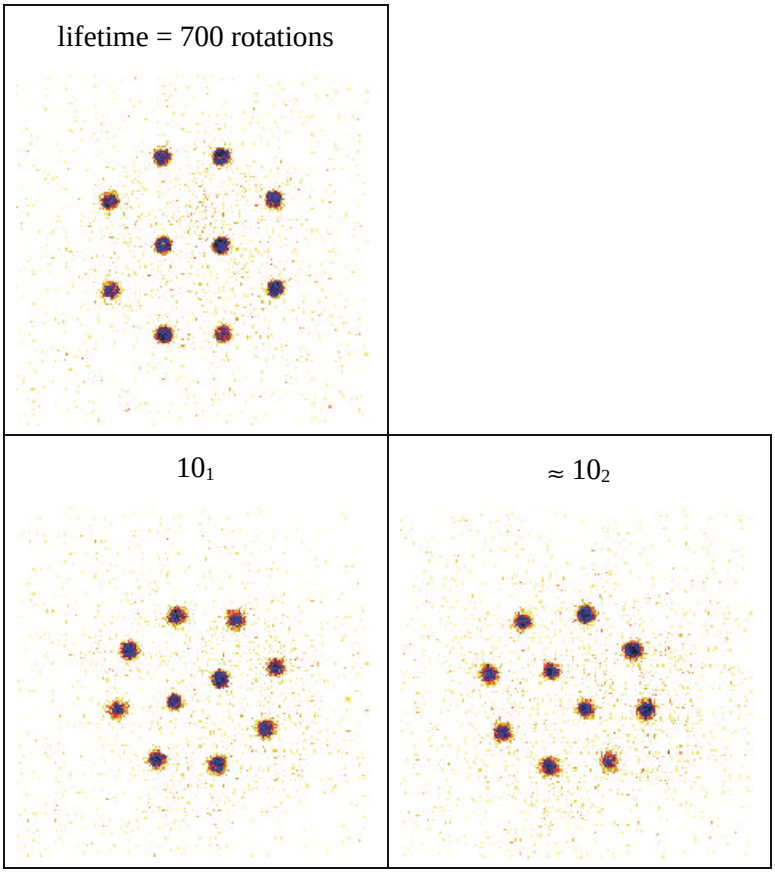

Figure 4.25: Campbell and Zi®'s 10_1.

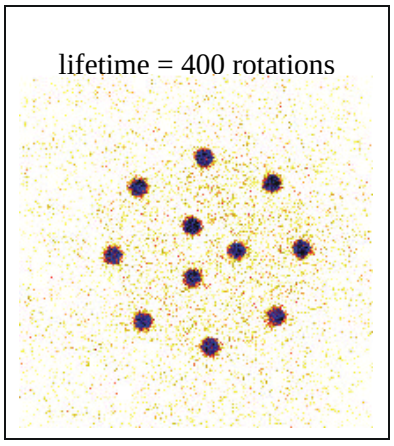

Figure 4.26: Campbell and Zi®'s 11_1.

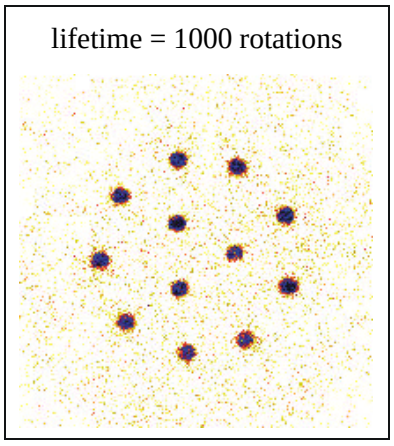

Figure 4.27: Campbell and Zi®'s 12_1.

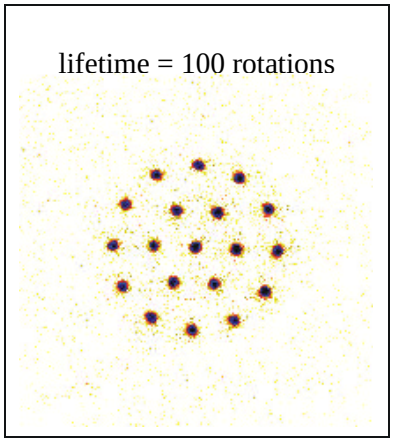

Figure 4.28: Campbell and Zi®'s 19_1.

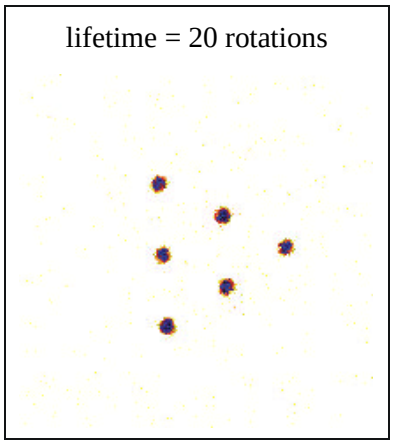

Figure 4.29: Jin's 6.

- Experiments on the stability of N vortices arranged in a ring, for N = 2 to 10, demonstrated excellent agreement with theory.
- Experiments on the stability of N vortices arranged in a ring with a central vortex, for N = 3 to 10, demonstrated good agreement with the theoretical stability limits on the central vortex's strength and excellent agreement with the theoretical mode of instability.
- The stability of more complicated vortex patterns from Campbell and Zi®'s catalog was explored, again with excellent agreement. Moreover, stable vortex patterns also found in Campbell and Zi®'s catalog emerged during the evolution of unstable patterns.

Given unlimited time and resources, I could have tested the stability of every single pattern in Campbell and Zi®'s catalog, totaling well over 100, and any other pattern one could dream up. As it was, the photocathode that generated most of the data in this thesis died, it proved impossible to resuscitate, and my work on 2D vortex patterns came to an end, at least for now.

Appendix A

The Fluid Analogy

There exists a powerful analogy between the electron systems in Malmberg-Penning traps and an ideal 2D °uid [57, 58, 59]. The analogy is based on the identical form of the 2D Drift-Poisson equations and the 2D Euler equations (see Table A.1). When certain experimental conditions are satis¯ed, the 2D Drift-Poisson equations will describe the evolution of an electron system in a Malmberg-Penning trap, and therefore this system will evolve identically as an ideal °uid.

The Fluid Analogy is valid under the following experimental conditions in a Malmberg-Penning trap:

- The guiding center approximation applies, meaning that the gyroradius is much smaller than any dynamical length scale of interest and that the gyrotime is much smaller than any dynamical time scale.
- The axial bounce time is much smaller than any dynamical time scale. This implies that an electron samples the entire axial region quickly compared to any dynamical time and can therefore be considered bounce averaged and two dimensional.
- The 2D motion is determined by E £ B drifts. This is really a \no viscosity" condition and eliminates ¯nite length e®ects and temperature dependent e®ects [60].

Note very importantly that there is nothing in the conditions about the electron system being a plasma. For the nonneutral plasma community, the adopted de¯nition of a plasma is a system where the Debye length is smaller than the size of the plasma. This condition

does not enter into The Fluid Analogy and therefore no such restriction is made on my experiments.

Because of The Fluid Analogy, Malmberg-Penning traps represent an excellent test bed for 2D °uid dynamics. Through the course of time, theoretical and computational °uid dynamics have outpaced experiments because of the challenges of controlling initial conditions and of the viscosity of real °uids. For instance, consider the problem of 2D vortex merger. Vortex merger has been the subject of much theorizing and simulating [61, 34, 62], but it is an experiment di±cult to perform with a real °uid. Experiments in rotating water tanks are fraught with viscosity and ¯nite length problems, as well as di±culty controllably creating the initial vortices [9]. The experiment, though, has been performed in a Malmberg-Penning trap at UCSD [13]. Malmberg-Penning traps can operate in a near-zero viscosity limit and now with the photocathode, the initial conditions are easily controlled. There is the added bonus that under the 2D Drift-Poisson equations, vorticity of the electron °uid is proportional to electron density. Vorticity is a quantity of fundamental importance in °uid dynamics, but di±cult to measure experimentally. In The Photocathode Trap, though, density in the form of line charge is measured with the CCD imaging system, and therefore so is vorticity. This is also the reason for calling a column of electrons in a Malmberg-Penning trap a vortex.

There have been a number of experiments that have exploited The Fluid Analogy to perform °uid-type experiments in Malmberg-Penning traps. Below are listed just a few:

- Symmetric vortex merger, also known as the Pairing Instability [13, 36].
- The Diocotron Instability, also known as the Kelvin-Helmholtz Instability [12].
- The Winding Instability for asymmetric rings [63].
- The relaxation of 2D turbulence [64, 18].
- The formation of stable vortex patterns, also called vortex crystals [18].
- Experiments with 2D vortex patterns, described within this thesis.

2D Drift-Poisson	2D Ideal Euler
E £ B Drift Velocity $v = -\frac{1}{B} r\Phi \times \hat{z}$	Stream Function Equation $v = -r^{\perp} \times \hat{z}$
Poisson Equation $r^2\Phi = \frac{e}{\epsilon_0} n$	Stream Function-Vorticity Equation $r^2 \omega = -$
Vorticity De¯nition $- = r \times v$ $= \frac{1}{B} r^2\Phi$ $= \frac{e}{\epsilon_0 B} n\hat{z}$ $- / n$	Vorticity De¯nition $- = r \times v$
Continuity Equation $\frac{\partial n}{\partial t} + v \cdot r n = 0$ $\frac{\partial -}{\partial t} + v \cdot r - = 0$	Momentum Equation $\frac{\partial \mathbf{v}}{\partial t} + v \cdot r v = -\frac{1}{\rho} r p$ $\frac{\partial -}{\partial t} + v \cdot r - = 0$
Conductive Wall $\Phi(\text{wall}) = \text{constant}$	Frictionless Wall $\omega(\text{wall}) = \text{constant}$

Table A.1: Note two items: 1) In the 2D Drift-Poisson system, the vorticity of the electron motions is proportional to the electron density; 2) The Continuity Equation and the Momentum Equation are identical in form, and therefore both systems evolve identically.

Appendix B

Magnetic Field Alignment Procedure

The misalignment of the magnetic ¯eld with the trap's axis is the prime suspect in the ¯nite lifetimes observed in Malmberg-Penning traps [39]. Also, The Fluid Analogy assumes that the magnetic ¯eld is purely axial. A number of procedures exist to align the magnetic ¯eld with the trap's axis and include the observation of electron con¯nement time and diocotron signals. In traditional traps with thermionic ¯laments, these procedures can be complicated by those sources being physically o®-center and producing nonuniform electron columns.

The Photocathode Trap o®ers an easy, direct way of aligning the magnetic ¯eld with the trap's axis:

1. Find the center of the trap on CCD images: The center of the trap can be found by fully illuminating the photocathode, producing a beam that ¯lls the trap and an image that reveals the trapping region. Measurements of this image can determine the center of the trap, and therefore also the center of the photocathode as it corresponds to the CCD image.

2. Inject a small radius electron column centered on the photocathode: Using the CCD imaging system, simply steer the light source such that the center of the photocathode is illuminated. This will produce an electron column that is being injected into the center of the trap.

3. Observe ` = 1 diocotron: If there is misalignment, an electron column injected at center will diocotron. Adjust the steering coils to suppress this motion. This will then align the magnetic ¯eld with the trap axis.

Appendix C

Electric Potential Pro¯le Control Option for the Photocathode

An original design goal for the photocathode injection system was the ability to control the electric potential pro¯le across the surface of the substrate. This goal was dictated by the belief that the electric potential at the cathode had to match the electric potential of the electron system in the trapping region, so that electrons would be uniformly injected [40]. It was discovered that at least in some limit, it was not necessary to control the cathode potential pro¯le and that a number of interesting experiments could be performed with an equipotential cathode. Because the control option is more complicated and tedious to install and because there were still many interesting experiments we could perform without it, it was removed from a later version of The Photocathode Trap. If the need ever arises, the option is presented here.

The electric potential control option is based on a system that uses a semi-transparent photocathode that is made in situ. The major challenge is establishing electrical contact with the emitting surface of the photocathode. With a transmission photocathode in general, indium tin oxide (ITO, a transparent conductor) coats the emitting surface for electrical contact. This easily makes an equipotential cathode by mounting the substrate into an electrically isolated holder.

To control the potential pro¯le, ITO pads are deposited on the surface instead of uniformly coating the substrate. The pattern depends on the design requirements and the calculation is based on the theory that the electron system's temperature is given by the

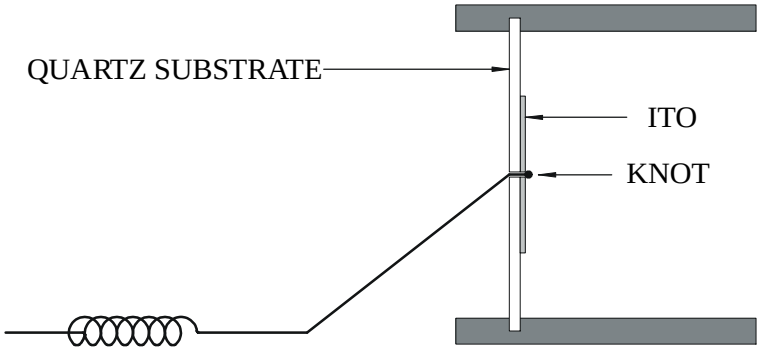

Figure C.1: Electrical contact is made with the ITO pad by feeding the tungsten wire through the laser drilled hole, knotting the wire, then spring loading it against the ITO pad.

potential mismatch. So for a given electron density, size column, and tolerable temperature, the pad placement can then be calculated.

The simplest version of the electric potential control option is diagramed in Figure C.1. To make contact with these pads, holes are laser drilled (performed by Laserage Technology) through the substrate and tungsten wire is fed through to the ITO pads. A simple knot is made in the wire and it is pulled back against the surface and spring loaded to a vacuum feedthru, out of the line of sight of the cathode. Some notes on the Electric Potential Control Option:

- In actuality, the holes are ¯rst laser drilled into the quartz substrate, then the ITO is deposited.
- A couple of control patterns were developed:
  - One was a pixelated version with the option of controlling 137 pads (see Figure C.2). A thin ITO layer of approximately 100 k-=2 is uniformly deposited over the substrate. Then, centered about the laser drilled holes, a thicker layer pad of ITO is deposited of approximately 100 -=2. This is to help establish electrical contact with the tungsten wire.
  - Another was a ringed version that essentially allowed for azimuthally symmetric electric pro¯les (see Figure C.3). As the radius of the rings increased, their radial thickness decreased to maintain a given potential mismatch. A uniform 100 -=2 coating of ITO was deposited on the substrate. Then, to make the

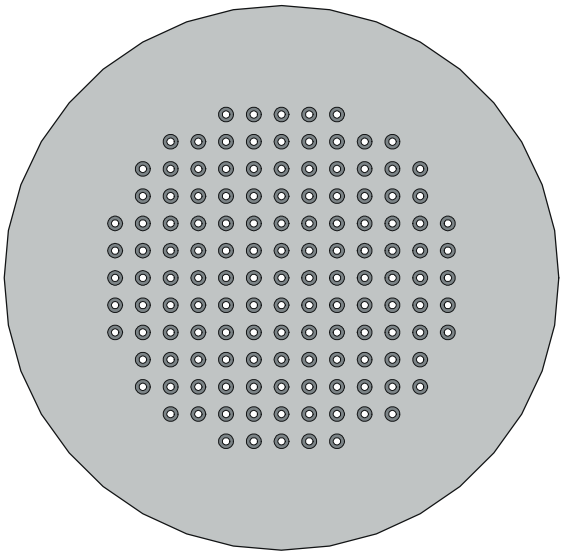

Figure C.2: The pixelated electric potential control version.

electrically isolated rings, the substrate was mounted on a rotatable stage in a milling machine. A \diamond dresser" was inserted in the chuck and allowed to just rest against the surface of the substrate. The dresser was positioned at the electrical conduction breaks and the substrate rotated, thereby etching away the ITO there and forming the electrically isolated rings.

- Amorphous quartz was used because of its ability to survive the laser drilling process. The quartz also had to be less than 1=16 of an inch thick to get cleanly drilled holes.
- The laser drilled holes were less than 0.010 inches in diameter and the tungsten wire was 0.075 mm in diameter.
- Beryllium copper springs were used because of their low magnetic susceptibility and ability to withstand a 200 $^{\pm}$C bake. They do become annealed above 200 $^{\pm}$C though.
- Care must be taking when spring loading the many tungsten wires. Too much spring force can have dramatic results, and did!

Figure C.3: The ringed electric potential control version.

Bibliography

[1] J. Sommeria, S. D. Meyers, and H. L. Swinney. Laboratory simulation of jupiter's great red spot. Nature, 331:689, 1988.

[2] P. S. Marcus. Numerical simulation of jupiter's great red spot. Nature, 331:693, 1988.

[3] J. Miller, P. Weichman, and M. C. Cross. Statistical mechanics, euler's equations, and jupiter's red spot. Phys. Rev. A, 45:2328, 1992.

[4] A. J. Chorin. Vorticity and Turbulence. Springer, New York, 1994.

[5] P. Minnhagen. The two-dimensional coulomb gas, vortex unbinding, and super°uid-superconducting ¯lms. Rev. Modern Phys., 59:1001, 1987.

[6] J. Miller. Statistical mechanics of euler equations in two dimensions. Phys. Rev. Lett., 65:2137, 1990.

[7] E. Caglioti, P. L. Lions, C. Marchioro, and M. Pulvirenti. A special class of stationary °ows for two-dimensional euler equations: A statistical mechanics description. Comm. Math. Phys., 143:501, 1992.

[8] E. G. Puckett. Vortex methods: An introduction and survey of selected research topics. In Incompressible Computational Fluid Mechanics, New York, 1993. Cambridge.

[9] R.W. Gri±ths and E.J. Hop¯nger. Coalescing of geostrophic vortices. J. Fluid Mech., 178:73, 1987.

[10] J. H. Malmberg, C. F. Driscoll, B. Beck, D. L. Eggleston, J. Fajans, K. Fine, X. P. Huang, and A. W. Hyatt. Experiments with pure electron plasmas. In C.W. Roberson and C.F. Driscoll, editors, Nonneutral Plasma Physics, volume AIP 175, page 28, New York, 1988. American Institute of Physics.

[11] J. Fajans and D. H. E. Dubin, editors. Non-Neutral Plasma Physics II, volume AIP 331. American Institute of Physics, New York, 1995.

[12] A. J. Peurrung and J. Fajans. Experimental dynamics of an annulus of vorticity in a pure electron plasma. Phys. Fluids A, 5:493, 1993.

[13] K. S. Fine, C. F. Driscoll, J. H. Malmberg, and T. B. Mitchell. Measurements of symmetric vortex merger. Phys. Rev. Lett., 91:588, 1991.

[14] L.J. Campbell and R. Zi®. A catalog of two-dimensional vortex patterns. Los Alamos Scienti¯c Laboratory Report No. LA-7384-MS, 1978.

[15] L.J. Campbell and R.M. Zi®. Vortex patterns and energies in a rotating super°uid. Phys. Rev. B, 20:1886, 1979.

[16] E.J. Yarmchuk, M.J.V. Gordon, and R.E. Packard. Observation of stationary vortex arrays in rotating super°uid helium. Phys. Rev. Lett., 43:214, 1979.

[17] E.J. Yarmchuk and R.E. Packard. Photographic studies of quantized vortex lines. J. Low Temp. Phys., 46:479, 1982.

[18] K.S. Fine, A.C. Cass, W.G. Flynn, and C.F. Driscoll. Relaxation of 2d turbulence to vortex crystals. Phys. Rev. Lett., 75:3277, 1995.

[19] T.H. Havelock. The stability of motion of rectilinear vortices in ring formation. Philos. Mag., 11:617, 1931.

[20] D.A. Schecter and D.H.E. Dubin. Dynamics of a single vortex in a nonneutral plasma. Bull. Am. Phys. Soc., 41:1604, 1996.

[21] R. Robert and J. Sommeria. Statistical equilibrium states for two-dimensional °ows. J. Fluid Mech., 229:291, 1991.

[22] R. Robert. A maximum entropy principle for two-dimensional perfect °uid dynamics. J. Stat. Phys., 65:531, 1991.

[23] B. Turkington and R. Jordon. Turbulent relaxation of a magneto°uid: A statistical equilibrium approach. In Advances in geometric analysis and continuum mechanics, pages 124{137, Boston, 1995. International Press.

[24] G.F. Carnevale, J.C. McWilliams, Y. Pomeau, J.B. Weiss, and W.R. Young. Evolution of vortex statistics in two-dimensional turbulence. Phys. Rev. Lett., 66:2735, 1991.

[25] G.F. Carnevale, J.C. McWilliams, Y. Pomeau, J.B. Weiss, and W.R. Young. Rates, pathways, and end states of nonlinear evolution in decaying two-dimensional turbulence: Scaling theory versus selective decay. Phys. Fluids A, 4:1314, 1992.

[26] R. Benzi, M. Colella, M. Briscolini, and P. Santangelo. A simple point vortex model for two-dimensional decaying turbulence. Phys. Fluids A, 4:1036, 1992.

[27] J.B. Weiss and J.C. McWilliams. Temporal scaling behaviour of decaying two-dimensional turbulence. Phys. Fluids A, 5:608, 1993.

[28] G. Huber and P. Alstrom. Universal decay of vortex density in two dimensions. Physica A, 195:448, 1993.

[29] D. G. Dritschel. Vortex properties of two-dimensional turbulence. Phys. Fluids A, 5:984, 1993.

[30] G. Riccardi, R. Piva, and R. Benzi. A physical model for merging in two-dimensional decaying turbulence. Phys. Fluids, 7:3091, 1995.

[31] P. Tabeling, S. Burkhart, O. Cardoso, and H. Willaime. Experimental study of freely decaying two-dimensional turbulence. Phys. Rev. Lett., 67:3772, 1991.

[32] O. Cardoso, D. Marteau, and P. Tabeling. Quantitative experimental study of the free decay of quasi-two-dimensional turbulence. Phys. Rev. E, 49:454, 1994.

[33] M. V. Melander, N. J. Zabusky, and J. C. McWilliams. Asymmetric vortex merger in two dimensions: Which vortex is 'victorious'? Phys. Fluids, 30:2610, 1987.

[34] H.B. Yao, N.J. Zabusky, and D.G. Dritschel. High gradient phenomena in two-dimensional vortex interactions. Phys. Fluids, 7:539, 1995.

[35] I.M. Lansky, T.M. O'Neil, and D.A. Schecter. A theory of vortex merger. Bull. Am. Phys. Soc., 41:1604, 1996.

[36] T. B. Mitchell. Experiments on electron vortices in a Malmberg-Penning trap. PhD thesis, University of California, San Diego, 1993.

[37] X. P. Huang, F. Anderegg, E. M. Hollmann, and C. F. Driscoll. Coherent vorticity holes from 2d turbulence decaying in a background shear °ow. Phys. Rev. Lett., 74:4424, 1995.

[38] A. E. H. Love. On the stability of certain vortex motions. Proc. London Math. Soc., 25:18, 1893.

[39] K. S. Fine. Experiments with the l=1 Diocotron Mode. PhD thesis, University of California, San Diego, 1988.

[40] J. H. Malmberg and J. S. deGrassie. Properties of a nonneutral plasma. Phys. Rev. Lett., 35:577, 1975.

[41] A. H. Sommer. Photoemissive Materials. John Wiley & Sons, Inc., New York, 1968.

[42] L. Holland. Vacuum deposition of thin ¯lms. Wiley, New York, 1956.

[43] A. J. Peurrung. Imaging of Instabilities in a Pure Electron Plasma. PhD thesis, University of California, Berkeley, 1992.

[44] A. J. Peurrung and J. Fajans. A pulsed, microchannel plate-based, nonneutral plasma imaging system. Rev. Sci. Instrum., 64:52, 1993.

[45] D. L. Eggleston, C. F. Driscoll, B. R. Beck, A. W. Hyatt, and T. H. Malmberg. Parallel energy analyzer for pure electron plasma devices. Phys. Fluids B, 4:3432, 1992.

[46] S. A. Prasad and T. M. O'Neil. Finite length equilibria of a pure electron plasma column. Phys. Fluids, 22:278, 1979.

[47] A. J. Peurrung and J. Fajans. Non-neutral plasma shapes and edge pro¯les. Phys. Fluids B, 2:693, 1990.

[48] C. F. Driscoll and J. H. Malmberg. Hollow electron column from an equipotential cathode. Phys. Fluids, 19:760, 1976.

[49] J. M. Kriesel and C. F. Driscoll. Electron plasma pro¯les from a cathode with an r^2 potential variation. Phys. Plasmas, 5:1265, 1998.

[50] William Thomson Kelvin. Mathematical and Physical Papers, iv. Cambridge University Press, 1878.

[51] J.J. Thomson. Treatise on Vortex Rings. Macmillan, London, 1883.

[52] D. G. Dritschel. The stability and energetics of corotating uniform vortices. J. Fluid Mech., 157:95, 1985.

[53] G.K. Morikawa and E.V. Swenson. Interacting motion of rectilinear geostrophic vortices. Phys. Fluids, 14:1058, 1971.

[54] L. J. Campbell. Transverse normal modes of ¯nite vortex arrays. Phys. Rev. A, 24:514, 1981.

[55] I.M. Lansky and T.M. O'Neil. Stability analysis of a two-dimensional vortex pattern. Phys. Rev. E, 55:7010, 1997.

[56] D.Z. Jin and D.H.E. Dubin. Maximum entropy theory of vortex crystal formation. Bull. Am. Phys. Soc., 41:1605, 1996.

[57] R. H. Levy. Diocotron instability in a cylindrical geometry. Phys. Fluids, 8:1288, 1965.

[58] R. J. Briggs, J. D. Daugherty, and R. H. Levy. Role of landau damping in crossed-¯eld electron beams and inviscid shear °ow. Phys. Fluids, 13:421, 1970.

[59] C. F. Driscoll and K. S. Fine. Experiments on vortex dynamics in pure electron plasmas. Phys. Fluids B, 2:1359, 1990.

[60] A. J. Peurrung and J. Fajans. A limitation to the analogy between pure electron plasmas and 2-d inviscid °uids. Phys. Fluids B, 5:4295, 1993.

[61] M. V. Melander, N. J. Zabusky, and J. C. McWilliams. Symmetric vortex merger in two dimensions: causes and conditions. J. Fluid Mech., 195:303, 1988.

[62] A. H. Nielsen, X. He., J. Juul Rasmussen, and T. Bohr. Vortex merging and spectral cascade in two-dimensional °ows. Phys. Fluids, 8:2263, 1996.

[63] A.J. Peurrung, J. Notte, and J. Fajans. Collapse and winding in an asymmetric annulus of vorticity. Bull. Am. Phys. Soc., 37:1803, 1992.

[64] X. P. Huang and C. F. Driscoll. Relaxation of 2d turbulence to a metaequilibrium near the minimum enstrophy state. Phys. Rev. Lett., 72:2187, 1994.